Organics preserved in anhydrous interplanetary dust particles: Pristine or not?

The Meteoritical Society

Meteoritics & Planetary Science 1–29 (2019)
doi: 10.1111/maps.13414

Organics preserved in anhydrous interplanetary dust particles: Pristine or not?

Queenie H. S. CHAN[1,2]*, Ian A. FRANCHI[1], Xuchao ZHAO[1], Alice STEPHANT[1], Ian P. WRIGHT[1], and Conel M. O'D. ALEXANDER[3]

[1]Planetary and Space Sciences, School of Physical Sciences, The Open University, Walton Hall, Milton Keynes MK7 6AA, UK
[2] Present address: Department of Earth Sciences, Royal Holloway University of London, Egham Surrey TW20 0EX, UK
[3]Department of Terrestrial Magnetism, Carnegie Institution of Washington, 5241 Broad Branch Road, NW, Washington, District of Columbia 20015, USA
*Corresponding author. E-mails: queenie.chan@open.ac.uk, queenie.chan@rhul.ac.uk.

(Received 14 March 2019; revision accepted 05 October 2019)

Abstract–The chondritic-porous subset of interplanetary dust particles (CP-IDPs) are thought to have a cometary origin. Since the CP-IDPs are anhydrous and unaltered by aqueous processes that are common to chondritic organic matter (OM), they represent the most pristine material of the solar system. However, the study of IDP OM might be hindered by their further alteration by flash heating during atmospheric entry, and we have limited understanding on how short-term heating influences their organic content. In order to investigate this problem, five CP-IDPs were studied for their OM contents, distributions, and isotopic compositions at the submicro- to nanoscale levels. The OM contained in the IDPs in this study spans the spectrum from primitive OM to that which has been significantly processed by heat. Similarities in the Raman D bands of the meteoritic and IDP OMs indicate that the overall gain in the sizes of crystalline domains in response to heating is similar. However, the Raman Γ_G values of the OM in all of the five IDPs clearly deviate from those of chondritic OM that had been processed during a prolonged episode of parent body heating. Such disparity suggests that the nonaromatic contents of the OM are different. Short duration heating further increases the H/C ratio and reduces the $\delta^{13}C$ and δD values of the IDP OM. Our findings suggest that IDP OM contains a significant proportion of disordered C with low H content, such as sp^2 olefinic C=C, sp^3 C–C, and/or carbonyl contents as bridging material.

INTRODUCTION

Pristine extraterrestrial material provides crucial information about the evolution of our solar system. About 2×10^6 kg of extraterrestrial material accreted by the Earth each year are submillimeter interplanetary dust particles (IDPs; Flynn 1989; Bradley 2003). Although most individual IDPs are between 5 and 15 μm in diameter, larger "cluster" particles (50–500 μm, 10–20% of collected IDPs) are present that are agglomerates of particles that break apart on contact with the collection surfaces (Bradley 2003). IDPs are small enough to be decelerated by the atmosphere and survive atmospheric entry without complete vaporization or severe heating (e.g., Love and Brownlee 1993). They generally have higher H/C ratios and are more enriched in the moderately volatile elements (e.g., P, K, Na, S) and C than chondritic meteorites (Thomas et al. 1994; Flynn et al. 1996). Some IDPs contain a high abundance of carbon (10 wt%, up to >45 wt% as reported by Thomas et al. 1994) that is significantly higher than the most carbon-rich meteorites (carbonaceous chondrites contain 2–5 wt% of carbon; Schramm et al. 1989). The "soft-landed" IDPs are delivered to the Earth's surface intact, and thus, they are a crucial contributor of carbonaceous compounds to the early Earth (Anders 1989). IDPs are captured before they reach the ground and are curated in an ultraclean (Class-100) laboratory at NASA Johnson Space Center (JSC). Therefore, they retain pristine information about the exogenous carbonaceous material that is uncontaminated and relatively unaltered by terrestrial

processes compared to meteorites recovered from various expeditions.

Two principal groups of IDPs—anhydrous chondritic porous (CP) IDPs and hydrous chondritic smooth (CS) IDPs—are recognized. Based on the fine-grained, porous morphology (e.g., Bradley and Brownlee 1986; Bradley 2003), high abundance of carbon (Thomas et al. 1994; Flynn et al. 1996), and the presence of submicron silicate glass with embedded metal and sulfides (GEMS; Bradley 1994), CP-IDPs are suggested to relate to short period comets. With a likely cometary origin, CP-IDPs have avoided parent body processes (e.g., aqueous and metamorphic activities) that are common to most other astromaterials with an asteroidal origin. While the fluffy CP-IDP morphology and mineralogy suggest a link to ice-rich parent bodies (Rietmeijer 2004; Zolensky et al. 2006), most anhydrous CP-IDPs exhibit spectral characteristics similar to those of primitive solar system objects such as outer P and D asteroids (Bradley et al. 1996; Vernazza et al. 2015), and the most carbon-rich CP-IDPs to comet-like outer asteroid (Bradley et al. 1996; Bradley 2003). Hence, CP-IDPs are potentially the best samples that retain information about the interstellar organic matter (OM) that was present in the solar nebula, and offer insights into the nature and synthetic pathway of the first OM formed in our solar system. CS-IDPs are composed predominantly of hydrated layer silicates such as smectite (Germani et al. 1990). Their hydrated mineralogy suggests that CS-IDPs come from parent bodies in which aqueous alteration has occurred such as Main Belt C-type asteroids (Bradley et al. 1996). Nevertheless, the boundary between CP- and CS-IDPs is challenged by the presence of a group of IDPs of which trace amounts of hydrous minerals were found intermixed within a dominantly anhydrous lithology (Rietmeijer 1991; Keller et al. 1992; Zolensky and Lindstrom 1992; Thomas et al. 1993; Nakamura et al. 2005). This group of "hybrid" IDPs was thought to represent anhydrous asteroids that had experienced some degree of aqueous alteration, or short period comets that had experienced a brief and nonpervasive aqueous alteration episode (Zolensky and Lindstrom 1992; Nakamura et al. 2005).

IDPs contain highly disordered carbon associated with amorphous aromatic units, such as polycyclic aromatic hydrocarbons (PAHs) and their alkylated derivatives, connected by abundant aliphatic and carbonyl (C=O) moieties as bridging material (e.g., Clemett et al. 1993; Flynn et al. 2003, 2004, 2013; Keller et al. 2004; Busemann et al. 2009). OM in primitive anhydrous IDPs is similar to that observed in acid residues of primitive chondritic meteorites; however, the aromatic/aliphatic ratio is notably lower in the IDPs (Flynn et al. 2003; Keller et al. 2004), which indicates the presence of abundant aliphatic bridges, heteroatoms, with high H/C ratios (Muñoz Caro et al. 2006). Clemett et al. (1993) showed that two of the eight IDPs they analyzed contain high-mass PAHs (500–700 atomic mass units [amu]), which could potentially reflect the presence of OM unique to IDPs, or it could be a sign of thermal alteration (polymerization/sintering of lower molecular weight compounds) as a result of atmospheric entry heating (Thomas et al. 1995).

The OM in CP-IDPs is typically enriched in the heavier stable isotopes of H and N. They display some of the largest enrichments of D measured in solar system materials (δD values up to ~30,000%; Busemann et al. 2009), and are accompanied by significant spatial heterogeneity of OM at micrometer scale (Messenger 2000; Keller et al. 2004; Quirico et al. 2005). As various astrochemical processes could lead to D enrichment, such as low-temperature ion-molecule reactions in both gas- and solid-phase species (Brown and Rice 1986; Millar et al. 1989; Charnley et al. 1997; Robert 2002) and photodissociation of PAHs in the diffuse interstellar medium (ISM; Aikawa and Herbst 2001; Sandford et al. 2001), the isotopic anomalies indicate that the IDP OM contains primordial solar system materials with an origin in the ISM, cold (10–100 K) molecular cloud, and/or outer regions of the protoplanetary disk (Messenger et al. 2003; Keller et al. 2004).

Despite the potential of IDPs for delivering pristine carbonaceous material to the Earth, they are typically frictionally heated at elevated temperatures (400–900 °C) for several seconds during their atmospheric entry (Flynn 1989; Sandford and Bradley 1989; Love and Brownlee 1991). Nevertheless, the fact that there are IDPs with primitive OM suggests that not all have experienced such high temperatures. Anhydrous cometary IDPs are more significantly influenced by atmospheric entry heating than asteroidal IDPs as the former have higher eccentricity and inclination and travel faster at perihelion, and thus arrive at the Earth's stratosphere at higher velocities (Flynn 1989; Jackson and Zook 1992; Brownlee et al. 1995). Any organics present should have been irreversibly altered or decomposed at these temperatures. For instance, the preferential decomposition of the thermally labile aliphatic bridges during atmospheric entry heating could have lowered the δD (Keller et al. 2004). In contrast, the host of the N isotopic anomalies, such as high-mass polyaromatic hydrocarbons containing nitrogen-bearing heterocycles (Clemett et al. 1993), is more refractory than the D-rich aliphatic material (Keller et al. 2004), leading to a preferential loss of D-rich labile hosts to

heating compared to the abundance of N isotopic anomalies. Therefore, atmospheric entry heating can ultimately alter the isotopic composition and the organic structure of the OM by modifying the relative abundance of the aliphatic and aromatic components. In order to understand the nature of the most primitive OM that was present in IDPs, it is imperative to systematically identify the heating they experienced during atmospheric entry and the effects this causes.

Heated stratospheric IDPs have common traits, such as the development of magnetite rims on sulfide and GEMS grains (Germani et al. 1990; Flynn et al. 1992; Keller et al. 1992), the loss of solar-wind noble gases (e.g., Flynn et al. 1992; Brownlee et al. 1995), normal bulk isotopic compositions (Floss et al. 2010), and the loss of solar flare ion tracks in crystalline silicates by heating at temperatures exceed 600 °C for several seconds (Fraundorf et al. 1982; Sandford and Bradley 1989). These characteristics were used in various studies to infer the degrees of atmospheric entry heating (e.g., Bradley et al. 1984; Sandford and Walker 1985; Flynn 1989; Sandford and Bradley 1989; Bradley 1994, 2003; Keller et al. 1996, 2004; Floss et al. 2010). However, as IDPs exhibit significant spatial heterogeneity, there is an uneven distribution of suitable silicate crystals for proper track identification. Infrared spectroscopy can be used to constrain the maximum temperatures experienced by IDPs where O–H bonds are present (Sandford and Walker 1985; Sandford and Bradley 1989); however, this is limited to hydrated silicates and is therefore not suitable for anhydrous IDPs. Various Raman cosmothermometers using the widths of the "disordered" band at ~1620 cm^{-1} have been developed for chondritic OM (e.g., Busemann et al. 2007; Homma et al. 2015). However, IDP OM is appreciably different from chondritic meteorite OM, and since cometary CP-IDPs may not have experienced asteroidal parent body heating, these chondritic OM cosmothermometers may not be applicable. It is crucial to identify a more vigorous technique to properly address the extent of atmospheric entry heating an IDP has experienced, not only to discern particles derived from asteroidal orbits as opposed to those from cometary orbits but also to better constraint their formation.

This article compares the structure of the OM in five IDP samples and insoluble organic matter (IOM) extracted from chondrites that belong to various groups, including primitive and thermally processed carbonaceous (Vigarano-like [CV], Mighei-like [CM], Renazzo-like [CR]) and ordinary chondrites (OC). In order to appropriately characterize the organic contents of the IDPs, and to study the distribution of organic components and their correlation to mineral phases within the particles, we have conducted a range of coordinated studies with Raman spectroscopy, scanning electron microscopy (SEM), and nanoscale secondary ion mass spectrometry (NanoSIMS). We will evaluate the heating extents of each IDP sample, identify and describe the OM in the least altered IDP sample, and discuss the effects of atmospheric entry heating on the organic components.

EXPERIMENTAL PROCEDURES

Sample Preparation

IDP Samples

Five IDPs (Rosslyn3, Drake3, Drake4, Balmoral3b, and Amberley3; Fig. 1; Table 1) were selected from the collection of IDPs at the Cosmic Dust Laboratory at NASA JSC. The two "Drake" particles in this study belong to the same cluster. They are from the Grigg–Skjellerup collection (GSC) of NASA JSC, which contains IDPs that were collected during the Earth's passage through the comet 26P/Grigg–Skjellerup's dust stream. The IDPs were retrieved from flat plate collection surfaces coated with silicone oil (dimethyl siloxane) flown aboard NASA ER-2 aircraft. Prior to distribution to the Open University (OU), the IDPs were individually removed from the collectors at NASA JSC using glass-needle micromanipulators, and were washed with hexane to remove the silicone oil. At OU, the samples were picked from the NASA glass slides by ©MicroProbes tungsten microneedles (<1 μm tip diameter) with a micromanipulator under an optical microscope objective, and pressed flat with a spectroscopic grade sapphire window into annealed high-purity gold foils mounted on aluminum stubs.

Meteoritic IOM Samples

The IOM samples were prepared by demineralization of the bulk meteorites with CsF-HF dissolution according to the methods described in Cody and Alexander (2005). They belong to a wide range of chondrite groups (CV, CM, CR, OC; Table 2) that cover a range of alteration extents. These residues have also previously been studied by Raman spectroscopy by Alexander et al. (2007), Busemann et al. (2007), and Starkey et al. (2013). The IOM residues were dispersed onto glass slides and directly analyzed by Raman spectroscopy.

Raman Spectroscopy

Raman spot analysis was the first technique used to analyze the IDP samples when they were still on the NASA glass slides using a Jobin-Yvon Horiba LabRam HR (800 mm) Raman microprobe at OU. The

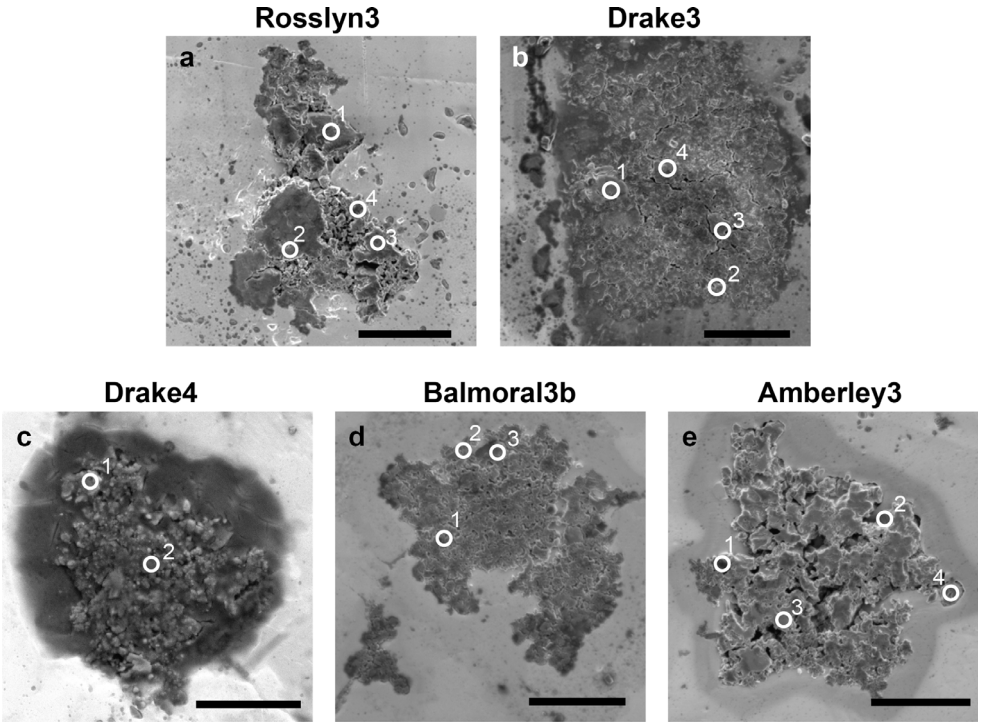

Fig. 1. High-resolution SE images of the IDP samples obtained by FE-SEM. Locations where EDX spot analyses were conducted were marked as numbered circles of which the elemental abundances are presented in Table S4 in supporting information. Scale bars are 5 μm.

Table 1. IDP sample numbers, sample names, associated collector and cluster, collector flight information, and size after pressing.

Sample #	Sample name	Collector	Cluster	Flight date	Flight duration (h)	Flight area	Particle size after pressing (μm)	Remarks
L2036-CA1	Rosslyn3	L2036	4	June 7 to July 5, 1994	26	California to Wallops Island, VA and on to New England	15.4 × 10.1	
L2055-T1	Drake3	L2055	5	April 30 to May 1, 2003	7.9	Over the southwestern USA	15.7 × 13.3	Grigg–Skjellerup collection
L2055-U1	Drake4	L2055	5	April 30 to May 1, 2003	7.9	Over the southwestern USA	10.3 × 8.4	Grigg–Skjellerup collection
L2071-K1	Balmoral3b	L2071	2	June 30 to July 30, 2008	50	Over the Eastern coast of the USA, the Great Lakes, and Canada	14.1 × 10.8	
L2076-Q1	Amberley3	L2076	7	April 27 to May 9, 2009	21.7	Off the California coast	13.5 × 13.3	

excitation source was a 514.53 nm (green) laser. The slit width and the confocal pinhole aperture were set at 150 and 200 μm, respectively, and a 600 grooves per mm grating was used to disperse the Raman signal, leading to a spectral resolution of approximately 3 cm^{-1}. The laser beam was focused through a microscope equipped with a 50× objective (numerical aperture = 0.75). At this magnification and for the laser used, the theoretical minimum achievable spot size of the Raman probe was approximately ~0.8 μm, and the laser power at the sample surface was ~60 μW. At least 30 spectra were collected for each IDP sample in the spectral range of 100 to 4000 cm^{-1}, which includes the first- (~1000 to 1800 cm^{-1}) and second-order (~2200 to 3400 cm^{-1})

Table 2. C Raman band parameters of the IDPs. Uncertainties are 1σ SD of the mean.

Samples		Find/ Fall	PMT (°C)*	G band (cm^{-1}) ω	G band (cm^{-1}) Γ	D band (cm^{-1}) ω	D band (cm^{-1}) Γ	I_D/I_G	*n*
IDPs									
L2036-CA1	Rosslyn3			1598.5 ± 3.5	125.4 ± 9.9	1364.4 ± 6.6	266.7 ± 23.4	0.714 ± 0.064	35
L2055-T1	Drake3			1593.3 ± 4.6	118.0 ± 8.7	1373.3 ± 5.1	260.8 ± 16.2	0.763 ± 0.06	66
L2055-U1	Drake4			1591.4 ± 2.5	136.2 ± 12.0	1366.9 ± 6.6	276.6 ± 20.5	0.711 ± 0.06	31
L2071-K1	Balmoral3b			1605.6 ± 3.5	128.1 ± 5.5	1355.6 ± 6.2	253.6 ± 11.2	0.866 ± 0.107	30
L2076-Q1	Amberley3			1613.5 ± 2.2	114.5 ± 4.7	1352.3 ± 3.2	207.9 ± 12.9	0.879 ± 0.047	35
Meteoritic IOM									
CV3 oxA	Allende	Fall	590	1606.9 ± 1.7	60.5 ± 1.3	1350.7 ± 0.5	69.0 ± 1.7	1.387 ± 0.027	25
CV3 oxB	Kaba	Fall	310	1608.7 ± 0.4	60.6 ± 0.8	1339.6 ± 0.5	146.0 ± 1.9	0.811 ± 0.006	20
CM2	Murchison	Fall	<240	1604.4 ± 1.4	93.8 ± 3.7	1350.8 ± 2.7	237.8 ± 13.4	0.78 ± 0.03	18
CM2	Bells	Fall	<240	1599.9 ± 3.0	95.8 ± 5.4	1359.8 ± 9.0	273.0 ± 22.0	0.767 ± 0.049	26
LL3.2	Krymka	Fall	290	1612.1 ± 0.6	75.9 ± 0.9	1347.1 ± 0.2	155.5 ± 1.4	0.885 ± 0.005	9
L3.05	QUE 97008	Find	250	1607.4 ± 5.5	86.1 ± 26.7	1353.2 ± 10.3	222.5 ± 26.4	0.737 ± 0.096	38
CR2	GRA 95229	Find	240	1600.6 ± 5.2	83.7 ± 7.0	1365.1 ± 8.6	251.8 ± 30.0	0.656 ± 0.065	57
CR2-an	Al Rais	Fall	220	1603.0 ± 4.9	78.5 ± 11.9	1365.2 ± 12.1	264.2 ± 32.8	0.63 ± 0.113	59

QUE = Queen Alexandra Range; GRA = Graves Nunataks.
*Peak metamorphic temperatures (PMT) are from Busemann et al. (2007) calculated based on the Γ_D of their OM.

Raman bands of carbon. The exposure time for each spectrum was 20 s and three accumulations were obtained for each analytical spot to identify and discard spurious signals, such as those from cosmic rays, leading to a total acquisition time of up to 180 s. Autofocus was applied prior to every analytical point on maximum Raman signal in the spectral region of 1580–1600 cm^{-1}, which broadly includes the first-order D and G bands. Peak position was calibrated daily against a silicon wafer prior to sample analyses and no significant shift was observed. Laser power was also checked daily prior to analyses to ensure that the laser power was consistent among all samples. Spectral peak identification and methods used in the present study were the same as outlined in Chan et al. (2017, 2019).

High-resolution Raman mapping was also conducted after the samples were pressed in gold and field emission gun (FEG) SEM characterization. Raman analyses were conducted prior to as well as after FEG-SEM analysis to investigate the e-beam C contamination artifacts. Further details on the experimental artifacts from C contamination are provided in the SEM C Contamination section and the supporting information. All the experimental parameters were maintained the same as for the low-resolution mapping and spot analyses on the glass slides, except for the spectral range, which was specified to include only the first-order Raman bands, from 500 to 2000 cm^{-1}. A step size of 0.5 μm in both the *x* and *y* directions was selected to approach the above-mentioned spatial resolution of 0.8 μm, leading to a total of at least 1000 spectra for each IDP sample. The sample surface was reexamined by the optical microscope to check for any damage and we confirm that no sign of physical damage was observed.

Curve-Fitting and Baseline Correction

The peak position (ω) and full width half-maximum (FWHM, Γ) of each Raman band were determined by simultaneous peak fitting to the two-peak Lorentzian and Breit–Wigner–Fano (BWF) model (Ferrari and Robertson 2000) and linear baseline correction. Details of the Raman peak fitting procedures and rationales are given (Chan et al. 2017, 2019; see supporting information for further details). Raman band parameters for each sample were reported as average of all selected spectra and the uncertainties are the 1σ standard error of the mean of all used spectra.

FEG-SEM Analysis

Electron images of the IDPs were obtained with an FEI Quanta 650 FEG-SEM at the Natural History Museum in London. The C distribution and elemental compositions of the IDPs were determined by energy dispersive X-ray microanalysis (EDX) using a Bruker XFlash FladQUAD 5060F detector. A low accelerating voltage was used for secondary electron (SE) imaging (2 kV) and EDX analysis (6 kV) to enhance the SE image resolution, analytical spatial resolution (<200 nm), and minimize beam damage/C contamination.

NanoSIMS Analysis

Isotopic imaging analysis was performed by a NanoSIMS 50L ion microprobe at OU in order to

determine the spatial distributions of the H, C, N, and O isotopes in the IDP samples. The NanoSIMS analysis was carried out by building on the methods described in Davidson et al. (2012), Starkey and Franchi (2013), and Chan et al. (2018). As the analytical methods have been reported in detail in these studies, only the key information is given below. Further details regarding analytical parameters and data processing are provided in the supporting information.

Isotopic images were acquired in multi collection mode with electron multipliers (EMs). The analyses were conducted in three analytical setups: (*Set-up 1: targeting C and N isotopes*) ^{16}O, $^{12}C^{12}C$, $^{12}C^{13}C$, $^{12}C^{14}N$, $^{12}C^{15}N$, $^{28}Si^{28}Si$ (*Set-up 2: targeting H isotopes*) ^{1}H, ^{2}H, ^{12}C, ^{13}C, ^{18}O; and (*Set-up 3: targeting O isotopes*) ^{16}O, ^{17}O, ^{18}O, ^{30}Si, $^{24}Mg^{16}O$, $^{56}Fe^{16}O$. A Cs^+ probe with a current of 2 pA for C and N isotopes, 4 pA for H isotope, and 1 pA for O isotope measurement was rastered over the samples with a raster size relevant to the particular particle being analyzed (Table S2 in supporting information). A frame size of 256 × 256 pixels was used for all images with an integration time of 1000 ms per pixel, leading to pixel step sizes of 50–66 nm. Planes of image data were corrected for detector dead time and combined, aligned, and processed using the L'image software (Larry Nittler, Carnegie Institution of Washington). Data were corrected for natural isotopic and instrumental mass fractionation (IMF) relative to the isotopic values of ~10 μm terrestrial standard 1-hydroxybenzotriazole hydrate (1-HOBt; assay ≥97.0%; $C_6H_5N_3O{\cdot}xH_2O$) for C, N, and H isotopes, and San Carlos olivine for O isotope measurements every day before and after the analytical run of the IDP samples (Table S3 in supporting information). Errors are reported as two standard deviations of the mean of multiple analyses (all image planes combined for each analysis; 2σ), which have taken into consideration the error based on counting statistics, the IMF, as well as the reproducibility of standards measured during the different analytical sessions over the course of this study. C/H ratios are reported here as corrected ion ratios $^{12}C/^{1}H$ with reference to the reported value (1.8) of the Drake particle (Davidson et al. 2012), and, hence, are rough estimates of the true C/H in bulk IDPs.

RESULTS

Grouping of the Heated and Unheated Anhydrous CP-IDPs

High-resolution SE, backscattered electrons (BSE) images, and EDX spectra were obtained for each IDP (Figs. 1 and 2). The IDP samples display bulk elemental compositions similar to that of chondritic materials (Zolensky et al. 1993; Table S4), and their mineralogy is comparable to that of anhydrous IDPs (Bradley and Brownlee 1986; Zolensky and Thomas 1995; Bradley 2003; Nakamura-Messenger et al. 2011). The five IDP samples are generally fine-grained and porous in texture, and are composed of fragile aggregates of predominantly sub-μm anhydrous minerals such as Mg-silicates (enstatite, forsterite) and low-Ni sulfides (pyrrhotite [$Fe_{0.92}S$–$Fe_{0.95}S$]; Table S4). In addition to SEM analysis, the Mg-rich composition of the silicates can be inferred from Raman spectroscopy. Raman spectra of olivine has a doublet at around 815–860 cm^{-1} that corresponds to the coupled symmetric ($í_1$) and asymmetric ($í_3$) vibrations of SiO_4 tetrahedra (Fig. 3, point C). The positions of the doublet peaks, although only clearly visible in Rosslyn3, can be used to estimate the Fo-Fa olivine composition (Kuebler et al. 2006), which confirms that the olivine in Rosslyn3 is forsterite ($Fo_{80\text{-}90}$; Fig. S3 in supporting information). Other minerals found in the samples include troilite (stoichiometric FeS) in Rosslyn3, Al-diopside in Amberley3, and high-Ni Fe-sulfides ($Fe_{0.6}Ni_{0.7}S$ pentlandite) in Drake3.

Although the IDP samples in this study have comparable mineralogy, one clear variation among the grains is the presence and abundance of magnetite. The Raman peaks around 670 and 540 cm^{-1} in Rosslyn3, Balmoral3b, and Amberley3 correspond to the A_{1g} mode of magnetite as a result of the symmetric stretch of oxygen atoms along Fe–O bonds, and the T_{2g} mode of the asymmetric stretch of Fe and O, respectively (Shebanova and Lazor 2003; Fig. 3, points D–G). These peaks are absent in the Drake particles. The relative intensity between the Fe–O (670 cm^{-1}) and C–C bands (1350–1380 cm^{-1}) in Amberley3 (points F and G) is higher than that of Rosslyn3 (points D and E), which serves as an indicator of the relative abundance of magnetite and C-bearing components. The locations of magnetite are often in association with the Fe-bearing phases such as sulfides, and the occurrence of magnetite is confined primarily to the particle surface. The development of such magnetite rims (<50 nm to ~2 μm thick) has been suggested to be the result of oxidation of Fe of Fe-rich phases. Peak temperatures of oxidation of sulfide are at 500–900 °C (Craig and Scott 1974), and oxidation of olivine at 600–1200 °C (Champness 1970; Rietmeijer 1996). Therefore, the presence of a magnetite rim has been used as one of the indicators of the severity of atmospheric entry heating in IDPs (e.g., Germani et al. 1990; Flynn et al. 1992; Keller et al. 1996) and micrometeorites (e.g., Greshake et al. 1998; Toppani et al. 2001; Suttle et al. 2017). The

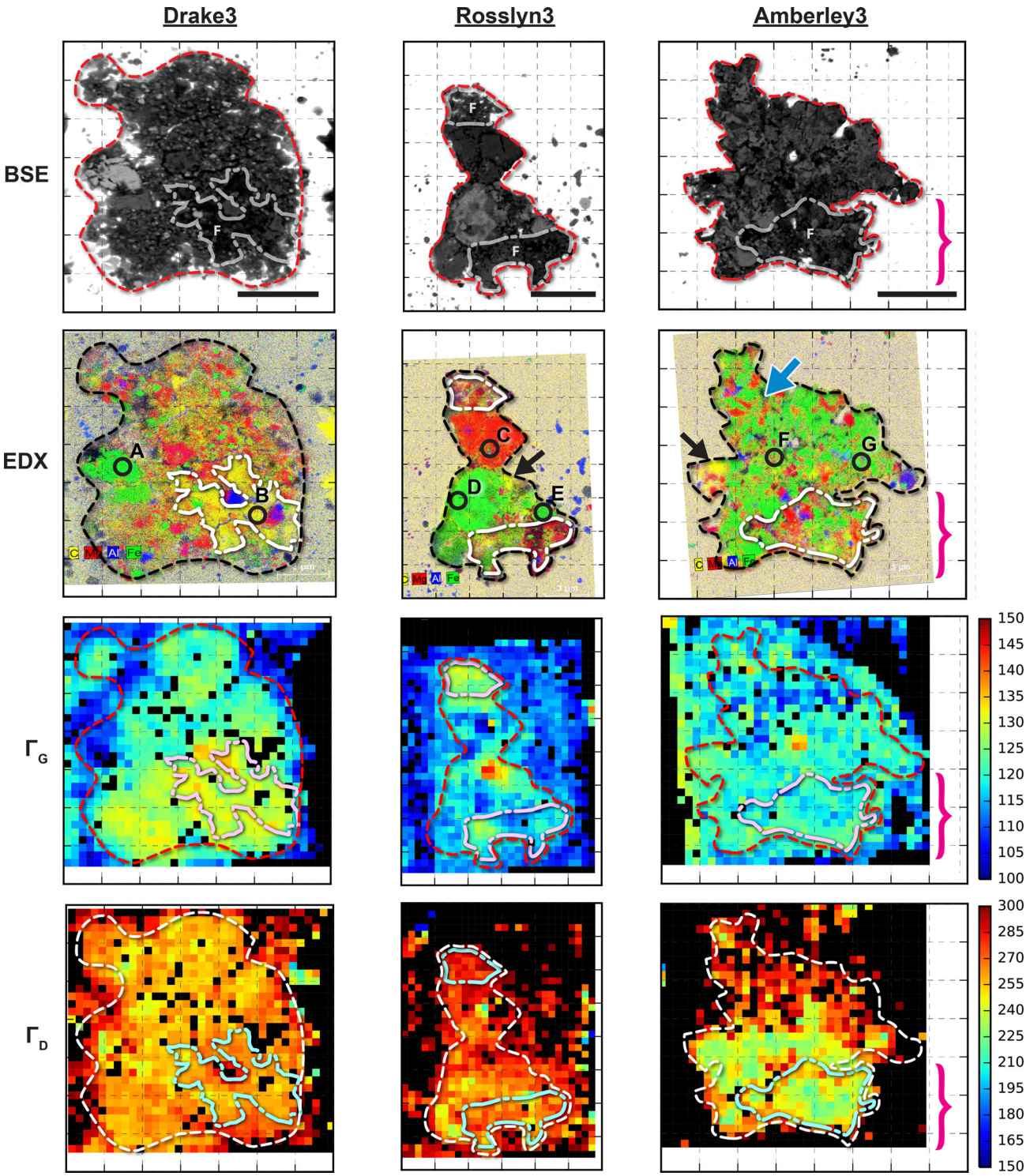

Fig. 2. BSE images, EDX combined C-Mg-Al-Fe X-ray maps (C is yellow, Mg is red, Al is blue, Fe is green), G FWHM (Γ_G), and D FWHM (Γ_D) Raman maps of Drake3, Rosslyn3, and Amberley3 which were obtained after SEM analysis. Black arrows indicate large, discrete C-rich grains (~0.5 μm in diameter). Blue arrow marks the occurrence of sulfide–silicate intergrowths in Amberley3 (shown as intermixed red [silicate] and green [sulfide] area in the combined X-ray map). Outlines of the particles are shown on the images to enhance the comparison between the maps. The fine-grained regions of the particles that appear in darker shade in the BSE images are marked by dash-dotted outlines. The C-rich region of Amberley3 is marked by the brackets. The region is more enriched in disordered OM as shown in the Γ_D map. Scale bars are 5 μm. Raman maps (pixel size: 0.5 × 0.5 mm^2). Raman spectra collected at Points A–G are shown in Fig. 3.

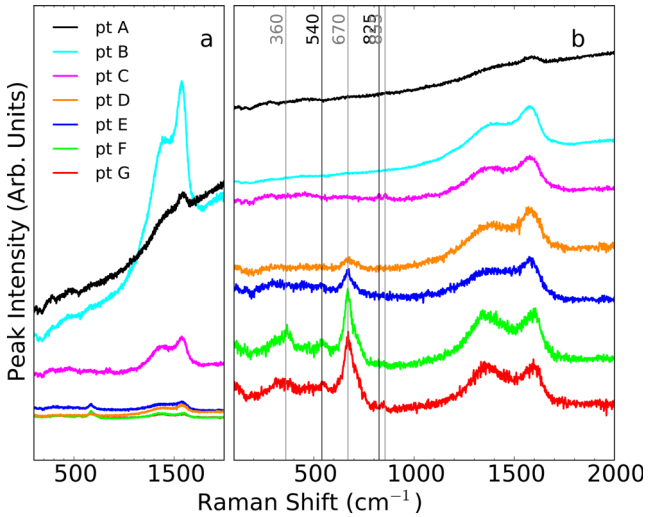

Fig. 3. Raman spectra of the IDP samples. Locations of the spots (A–G) are marked on the EDX maps in Fig. 2: a) Raw Raman spectra. b) Spectra normalized with respect to the maximum Raman intensity within the spectra range from 1580 to 1600 cm^{-1}. A vertical offset was applied to enhance the readability of the plots. Vertical lines mark the locations of the typical Raman D and G peaks, and peaks of olivine doublet around 825 and 855 cm^{-1} and magnetite around 540 and 670 cm^{-1} (Shebanova and Lazor 2003).

polycrystalline nature of the magnetite rim formed by atmospheric entry heating is clearly distinct from the typical crystal forms (framboids, plaquettes, and spherules) taken by magnetites formed by aqueous processes (Chan et al. 2016). The absence of any magnetite rim in Drake suggests that it has been exposed to the least heating compared to the other three IDPs in this study.

Based on the texture and the heating extent experienced, we have subclassified the five IDP samples in this study into three types: *Type I IDPs* are dominated by fine-grained (<0.5 μm), porous, heterogeneous aggregates of crystalline mineral grains and carbonaceous materials (Drake3, Drake4, Balmoral3b; Figs. 1b–d) which are relatively unheated without magnetite development; *Type II IDP* is moderately heated (the ratio between the peak intensities of the magnetite at ~670 cm^{-1} and Raman C defect band at ~1350–1380 cm^{-1} [I_{mag}/I_D]) ≤1) and contains coarse-grained enstatite and Fe-Ni metal (>3 μm) with a fine-grained, porous matrix (Rosslyn3; Fig. 1a); *Type III IDP* is extensively heated (I_{mag}/I_D >1) and contains medium-grained (~1 to 1.5 μm) sulfide–silicate intergrowth with a fine-grained, porous matrix (Amberley3; Fig. 1e). The sulfide–silicate intergrowth has also been observed in the comet 81P/Wild 2 samples and CP-IDPs that belong to large clusters, which were believed to have formed by thermal metamorphic processes in the nebula (Joswiak et al. 2009).

SEM C Contamination

When imaging at high magnifications, SEM analysis can deposit C onto the electron-irradiated sample surface, due to the cross-linking of adsorbed organic molecules under electron irradiation (Hart et al. 1970; Hirsch et al. 1994; Antognozzi et al. 1997). The deposited C, of which the C Raman features are visible outside the IDP samples in the Raman maps (Fig. 2), is composed of light hydrocarbons which were formed by cracking of large, complex precursors. The hydrocarbon film contamination is homogenous and has a similar Raman spectral feature as disordered C, thus leading to clustering of Raman peak parameters and increasing the disordered bandwidth (Fig. S5 in supporting information). Therefore, for intersample comparison, only Raman spectra that were obtained prior to SEM analysis were considered. Further discussion on the experimental artifacts from C contamination is provided in the supporting information.

Raman Observations of IDP OM

Carbonaceous materials feature Raman bands in the first- and second-order regions. The most typical peaks are the first-order defect (D) band at ~1350 to 1380 cm^{-1} and the graphite (G) band at ~1580 to 1590 cm^{-1} (Tuinstra and Koenig 1970). The high-resolution SEM-EDX and Raman analyses show in detail the relationship between the C-containing phases and the mineralogy of the five IDP samples in this study (Fig. 2).

While the C-rich phases often occur in the matrix as fine-grained material around silicate grains (Fig. 2), which echoes with previous description of the OM as the "glue" that holds the mineral grains together (Flynn et al. 2003, 2013), some occur as discrete C-rich grains (~0.5 μm, marked by arrows in Fig. 2). The majority of the Raman spectra is dominated by those that exhibit Raman C bands accompanied by strong fluorescence signature (Fig. 3a). A reduction in the fluorescence background intensity was observed for the OM in Rosslyn3 and Amberley3 (points C–G) relative to that in Drake3 (points A and B). Despite the abundance of crystalline silicate phases in IDPs, such as olivines that have sharp distinctive peaks, they are not observed in most of the Raman spectra of IDPs in the literature as well as in this study. This is due to the low laser power that led to a very weak Raman silicate signal relative to the carbonaceous material. However, similar observations have led Wopenka

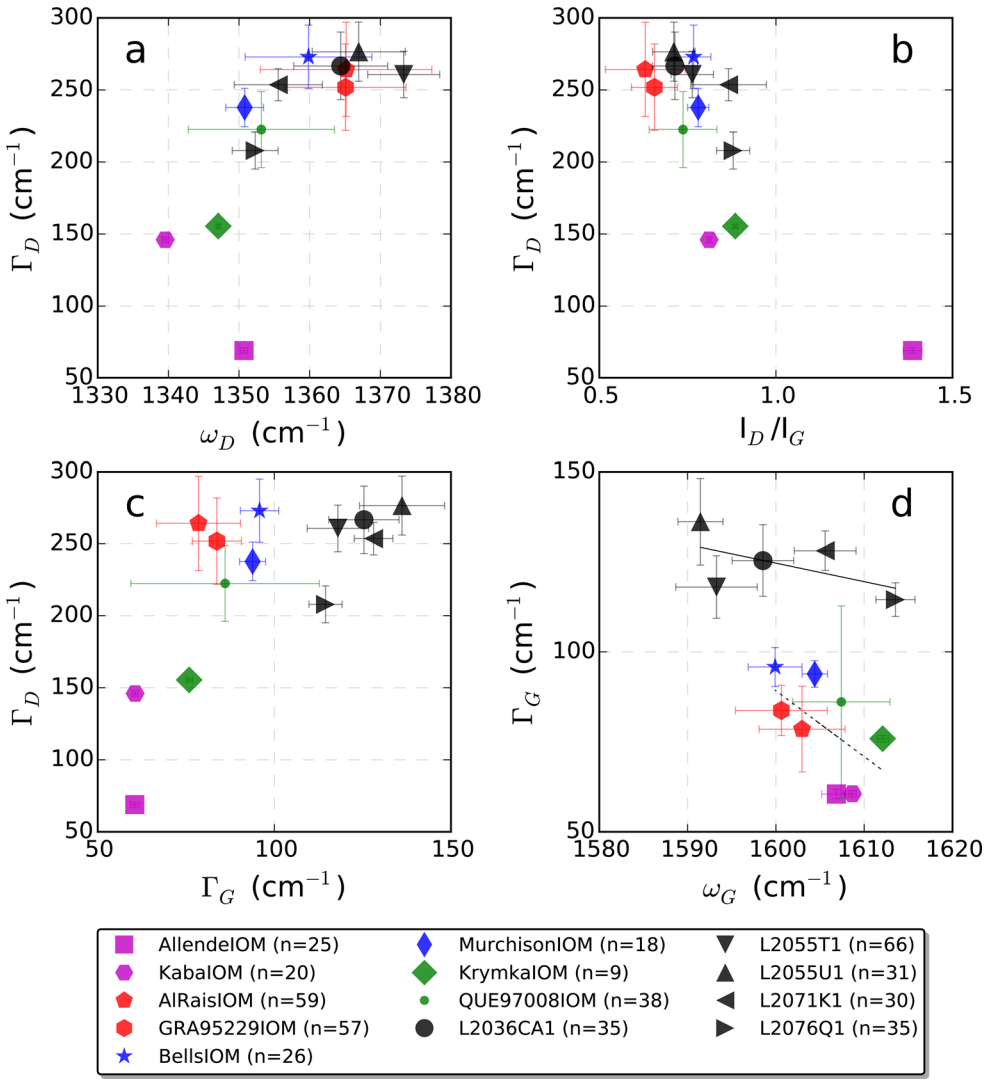

Fig. 4. Comparison of the Raman D and G band parameters (ω = peak center locations, Γ = full-width half-maximum, I_D/I_G = peak intensity ratios between the D and G bands) of the OM in the IDP samples (black markers) and chondritic IOM (blue = CM; green = OC; red = CR; magenta = CV). The values were obtained by peak fitting to the two-peak Lorentzian and BWF model and linear baseline correction. The G band parameters in subplot (d) of chondritic and IDP OM are notably different. The slopes of the trend lines of chondritic IOM and IDP OM in subplot (d) are −1.8 and −0.5, and the R^2 values are 0.321 and 0.305, respectively. Uncertainties are 1σ standard deviation (SD) of the mean.

(1988) to conclude that the silicates are coated by carbonaceous material.

The Raman parameters of the OM in the five IDPs in this study and chondritic IOM are listed in Table 2, and the data are plotted in Figs. 4–6 to illustrate the peak parameter correlations. The degree of intraparticle heterogeneity within the IDP OM is shown in Fig. S2 in supporting information. Individual data points in Fig. S2 are from the individual spectra obtained from the Raman maps, which were used to produce the average values reported in Table 2; Figs. 4–6. The clustering of the Raman parameters is also represented by the small error bars (1σ standard deviation) in Fig. 4, which not only suggests the reproducibility of the measurements but also indicates limited OM heterogeneity as a result of the irreversible annealing effect that homogenized the OM.

The Raman parameters of the OM in the IDPs in this study form a continuum that spans the more primitive to the more heated (less primitive) OM. The D band parameters of the OM in the five IDPs (ω_D = 1352–1373 cm^{-1}; and Γ_D = 208–277 cm^{-1}) are comparable to that of the IOM in CM and CR chondrites (ω_D = 1351–1365 cm^{-1}; and Γ_D = 238–

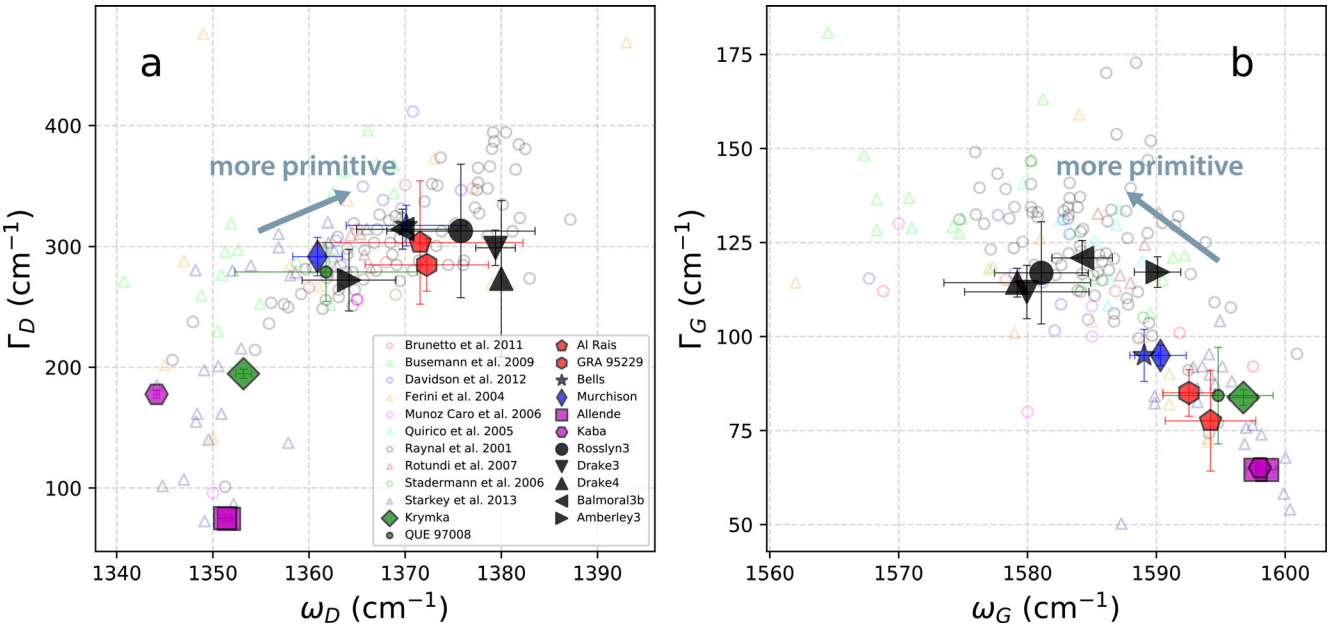

Fig. 5. Comparison of the Raman D and G band parameters of chondritic IOM, OM in the IDPs in this study, and OM in the IDPs reported in previous studies (Raynal et al. 2001; Ferini et al. 2004; Quirico et al. 2005; Muñoz Caro et al. 2006; Stadermann et al. 2006; Rotundi et al. 2007; Busemann et al. 2009; Brunetto et al. 2011; Davidson et al. 2012; Starkey et al. 2013). In order to facilitate the comparison between data reported in different studies, a two-Lorentzian peak fitting model was used to reprocess the data in this study. Thus, all data shown in this figure are acquired with the use of a two-Lorentzian peak fitting model. Busemann et al. (2009) and Stadermann et al. (2006) analyzed the IDP samples with a 532 nm laser. As lower ω_D and ω_G values are expected for analyses obtained with a 532 nm laser compared to a 514 nm laser (Ferrari and Robertson 2000), upshifts of 5 cm^{-1} were applied to the ω_D and ω_G values reported in these two studies (Rotundi et al. 2008). Uncertainties are 1σ SD of the mean.

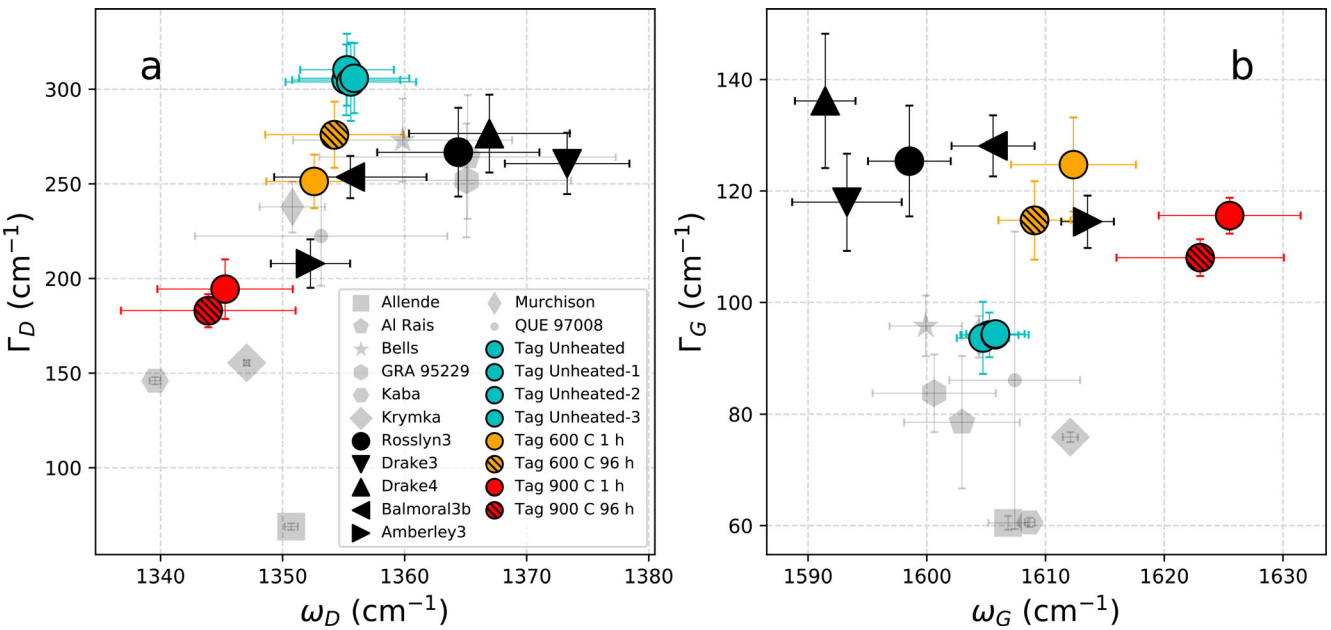

Fig. 6. Comparison of the Raman D and G band parameters of the OM in the IDPs to the OM in heating experimental products of the Tagish Lake meteorite and chondrites. Data of the Tagish Lake meteorite heating experimental products were obtained from Chan et al. (2019). Uncertainties are 1σ SD of the mean.

273 cm^{-1}; Table 2) and they share a similar maturity trend (Fig. 4). The D and G band parameters of the OM in the five IDPs are also comparable to that reported for other IDPs in the literature (Fig. 5).

With higher ω_D and Γ_D values, the OM in the GSC Drake particles presents the most disordered (least heated) among the five particles studied. With a higher ω_G (1614 cm^{-1}) and lower Γ_D (208 cm^{-1}), the OM in Amberley3 is clearly distinct from the other IDP samples (ω_G = 1591–1606 cm^{-1}; Γ_D = 254–277 cm^{-1}; Fig. 4; Table 2). The mineralogy, particularly with the presence of magnetite rims, and the degree of OM structural order of Amberley3 indicate that the particle has been extensively heated. The intraparticle clustering in Raman parameters is more prominent in Amberley3 compared to other IDP samples (Fig. S2), which further supports the interpretation that its OM has been more severely heated and homogenized. The Γ_D map of Amberley3 (Fig. 2) suggests that the structural alteration of the OM corresponds to the particle texture and mineralogy —the fine-grained region (as marked by the brackets in Fig. 2) is more enriched in OM, but the OM has been annealed by the heating process. The maturity of the OM in Rosslyn3 is intermediate (Fig. 4), which suggests that the particle has been heated to a moderate extent. This view is supported by previous observations of the development of minor magnetite rims alongside the presence of solar flare tracks (~10^{11} tracks per cm^2) in large olivine grains in particles from the same IDP cluster (Messenger et al. 2010; Nakamura-Messenger et al. 2012).

Although the Raman D parameters of IDP OM follow the maturity trend observed for chondritic OM and the data are plotted in the same area (Fig. 4a), the G band widths of IDP OM clearly deviate from that of chondritic OM (Figs. 4c and 4d). The Γ_G of IDP OM is at least ~18 cm^{-1} wider than that of chondritic OM. The variation in the G band components between IDP and chondritic OM has been noted in the past (Raynal et al. 2001; Quirico et al. 2005; Busemann et al. 2009; Brunetto et al. 2011; Starkey et al. 2013). Although the interpretation of such variation in terms of chemical composition is not straightforward (Quirico et al. 2005), it was suggested to likely indicate different concentrations of heteroatoms and the presence of extremely primitive OM in the IDPs (Busemann et al. 2009; Starkey et al. 2013).

Bulk Isotopic Compositions

The C, H, N, and O isotope mapping analyses performed in this study are presented in Fig. 7, and the isotopic compositions are presented in Table 3 and plotted on Figs. 8 and 9. The isotopic compositions of the IDP samples in this study are comparable to data reported in the literature (Fig. 9). Significant spatial heterogeneity has been observed for the carbonaceous material in the IDPs. The C-rich phases are shown as the darker regions in BSE images (marked as dash-dotted outline in Fig. 2), yellow colored regions in the EDX combined C-Mg-Al-Fe X-ray maps (Fig. 2), areas showing the typical Raman D and G bands (Fig. 2), and the ^{12}C-enriched areas in NanoSIMS ion images (Figs. 7c and 7m). In general, the C-rich areas in all five IDP samples have higher δD values; lower $\delta^{13}C$, $\delta^{15}N$ values; and H/C ratios than the sample bulk (Table 3; Fig. 9). Several D, ^{13}C, and ^{15}N isotopic anomalies (hotspots) possibly associated with OM were identified in Drake3 and Balmoral3b (δD = +4494 to +7012‰; $\delta^{13}C$ = +47‰; $\delta^{15}N$ = +3790‰; Table 3; Fig. 10). We did not observe any particular difference in the Raman spectra of the hotspots compared to that of the rest of the sample.

The textural affinity among the type I IDPs (Drake3, Drake4, and Balmoral3b) is accompanied by their similar bulk isotopic values, but their N isotopic compositions are less comparable (Table 3 and Fig. 9). GSC-IDPs are typically enriched in ^{15}N while such enrichment attests for their exogenous and primitive nature (Messenger 2000; Busemann et al. 2009; Davidson et al. 2012; Starkey et al. 2013). The bulk isotopic composition of Drake3 stands out from the rest of the IDP samples in this study, and is enriched in both D and ^{15}N (δD ≈ +739‰; D/H ≈ 0.0003; $\delta^{15}N$ ≈ +907‰; $^{15}N/^{14}N$ ≈ 0.007). The bulk $\delta^{15}N$ value of Drake3 is higher than that of all GSC-IDPs studied by far ($\delta^{15}N$ = –190 to +485‰), but its D enrichment is less prominent (the bulk δD values of typical GSC-IDPs = +190 to +8700‰; Busemann et al. 2009; Davidson et al. 2012).

The bulk O isotopic compositions of the IDPs fall within error of the slope = 1 line (Young and Russell 1998) with $\delta^{17}O$ values of –1.5 to +18.6‰ and $\delta^{18}O$ values of –4 to +14.5‰ (Table 3 and Fig. 8a). We have located three presolar silicate grains in Drake4, one in Amberley3, and three in Balmoral3b.

DISCUSSION

The Mineralogy, Processing, and Origin of Primitive IDPs

Previous studies of IDPs from clusters such as Rosslyn (L2036 Cluster 4; e.g., Aléon et al. 2006; Messenger et al. 2007, 2009, 2010; Nakamura-Messenger et al. 2012), Drake (L2055 Cluster 5; e.g., Davidson et al. 2012; Starkey and Franchi 2013), and Balmoral (L2071 Cluster 2; e.g., Starkey et al. 2014) indicate that they are anhydrous CP-IDPs. The absence

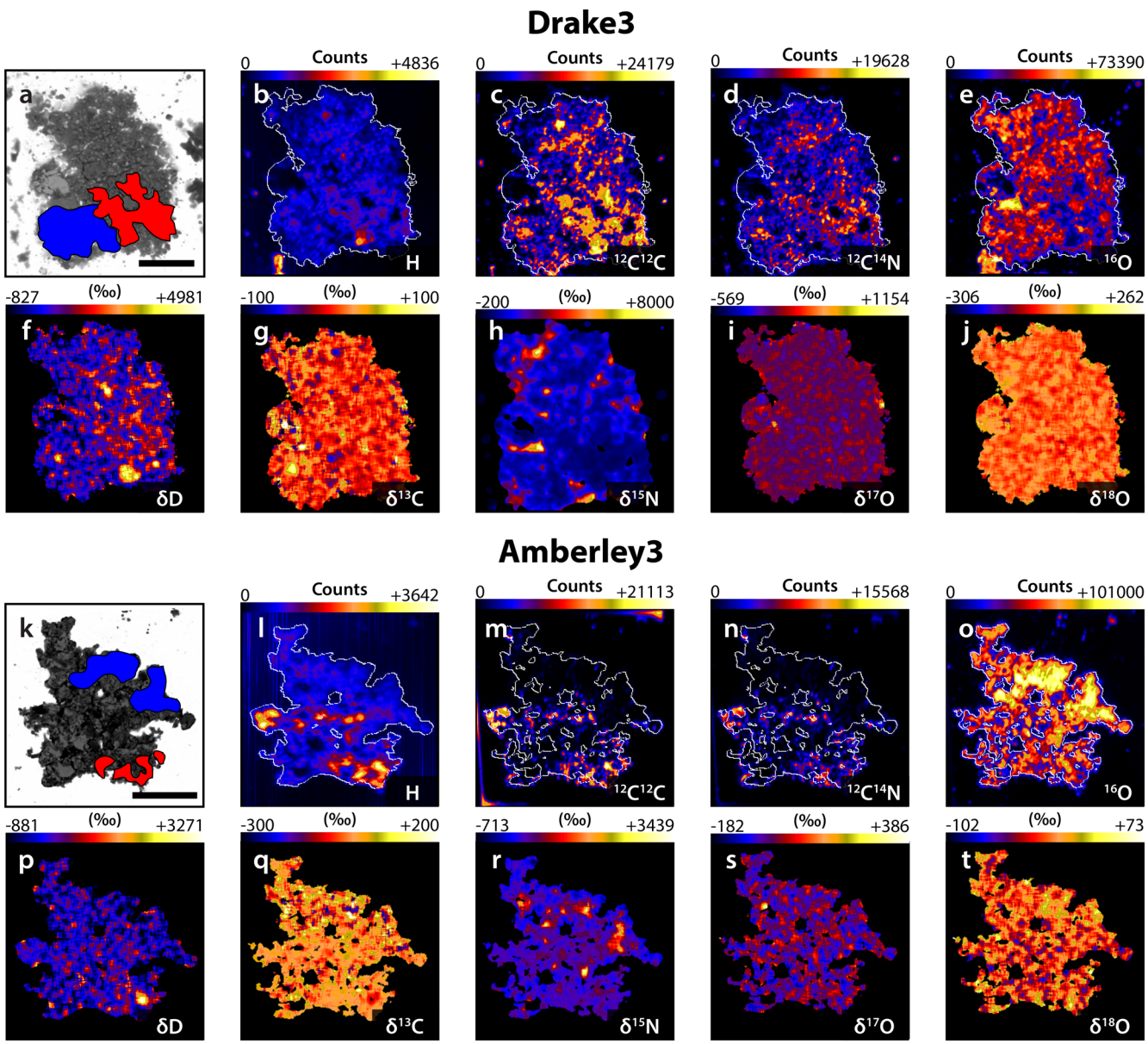

Fig. 7. (a, k) BSE images, NanoSIMS ion images of (b, l) H, (c, m) $^{12}C^{12}C$, (d, n) $^{12}C^{14}N$, and (e, o) ^{16}O, and isotope maps of (f, p) δD, (g, q) $\delta^{13}C$, (h, r) $\delta^{15}N$, and (i, j, s, t) $\delta^{17,\ 18}O$ of Drake3 and Amberley3. Isotopic compositions are reported as δ values, representing the deviations of the measured isotopic ratios from terrestrial values in per mil (‰), and are corrected for instrumental mass fractionation. Areas corresponding to C-rich and C-poor regions in Table 3 are highlighted red and blue, respectively, in subplots (a and k). Scale bars are 5 μm.

of aqueous alteration texture and mineral products (e.g., carbonates, phyllosilicates) in the IDP samples makes a hydrous/asteroidal origin less likely for the IDPs in this study. Although IDPs of mixed mineralogy (e.g., some "anhydrous" IDPs contain "hydrated" phases such as smectite) have been reported in the literature (Rietmeijer 1991; Keller et al. 1992; Zolensky and Lindstrom 1992; Thomas et al. 1993; Nakamura et al. 2005), the IDPs analyzed in this study are unlikely "hybrid" IDP based on our textural and mineralogy observations, and the interpretations made by other studies in the past. The texture of CP-IDPs tend to be "fluffy" or "porous," while that of CS-IDPs is generally described as being "smooth" or "compact." The morphology, surface microstructures, texture, and composition (based on FEG-SEM imaging) of the IDP samples in this study are consistent with that of anhydrous CP-IDPs. The high C/H ratio (>1) is also typical for CP-IDPs as opposed to the low C/H ratio (<1) in CS-IDPs (Schramm et al. 1989; Starkey and Franchi 2013).

Table 3. Carbon, hydrogen, nitrogen, and oxygen isotope results for IDPs in this study.[a]

Samples	Isotopic compositions (‰)						H/C[d]	ROI area (μm^2)
	δD	$\delta^{13}C$	$\delta^{15}N$	$\delta^{17}O$	$\delta^{18}O$	$\Delta^{17}O$[c]		
IDPs								
Rosslyn3								
Bulk	14 ± 82	−34 ± 2	451 ± 6	6 ± 5	2 ± 2	5 ± 5	1.5 ± 0.5	57.4
Enstatite	208 ± 136	−23 ± 4	382 ± 16	7 ± 6	−7 ± 3	11 ± 6	1.4 ± 0.4	12.4
Kamacite	−9 ± 117	−41 ± 5	873 ± 19	−5 ± 7	−1 ± 3	−4 ± 7	2.2 ± 0.7	8.7
Fe-rich	−188 ± 119	−43 ± 12	1282 ± 33	−7 ± 8	−16 ± 3	2 ± 8	5.4 ± 1.7	4.0
C-rich	−64 ± 86	−43 ± 3	379 ± 8	9 ± 6	8 ± 2	5 ± 6	1.2 ± 0.4	21.4
C-rich	610 ± 370	−18 ± 6	133 ± 45	9 ± 6	8 ± 2	5 ± 6	0.5 ± 0.1	0.5
Drake3								
Bulk	739 ± 128	−15 ± 1	907 ± 4	−1 ± 5	2 ± 2	−1 ± 5	0.6 ± 0.2	148.4
C-rich	1468 ± 189	−16 ± 1	482 ± 5	3 ± 9	1 ± 4	2 ± 9	0.5 ± 0.1	15.6
$\delta^{13}C$ hotspot	1820 ± 374	47 ± 5	1001 ± 19	−4 ± 25	13 ± 11	−10 ± 26	0.6 ± 0.2	0.8
$\delta^{15}N$ hotspot	173 ± 165	−12 ± 8	3791 ± 36	−25 ± 11	−7 ± 5	−21 ± 12	1.7 ± 0.5	2.4
C-poor	342 ± 111	−13 ± 2	1010 ± 7	3 ± 6	2 ± 3	2 ± 6	0.8 ± 0.2	23.8
Drake4								
Bulk	319 ± 97	−7 ± 1	183 ± 3	6 ± 5	−4 ± 2	8 ± 5	0.7 ± 0.2	60.1
C-poor	315 ± 97	−5 ± 1	211 ± 3	5 ± 5	−4 ± 2	8 ± 5	0.7 ± 0.2	54.2
C-rich	337 ± 108	−13 ± 1	29 ± 5	16 ± 9	0 ± 4	16 ± 10	0.6 ± 0.2	6.0
$\delta^{17}O$ hotspot	1240 ± 862	−35 ± 24	103 ± 50	1061 ± 58	5 ± 18	1058 ± 59	0.8 ± 0.3	0.1
$\delta^{17}O$ hotspot	1064 ± 856	−42 ± 18	169 ± 57	488 ± 57	−2 ± 20	489 ± 58	0.6 ± 0.2	0.1
$\delta^{17}O$ hotspot	−572 ± 304	17 ± 19	300 ± 48	905 ± 60	−32 ± 19	922 ± 61	0.7 ± 0.2	0.1
Balmoral3b								
Bulk	536 ± 115	−21 ± 1	159 ± 4	19 ± 5	14 ± 2	11 ± 5	0.5 ± 0.2	66.8
small particle	−236 ± 106	−12 ± 4	93 ± 17	28 ± 11	39 ± 5	8 ± 11	1.3 ± 0.4	3.2
$\delta^{17}O$ hotspot	−698 ± 215	−23 ± 11	105 ± 50	322 ± 41	−35 ± 15	341 ± 42	0.6 ± 0.2	0.2
$\delta^{17}O$ hotspot	243 ± 628	16 ± 13	154 ± 50	413 ± 56	−53 ± 20	441 ± 57	0.5 ± 0.1	0.1
$\delta^{18}O$ coldspot	−698 ± 215	−12 ± 12	151 ± 46	−72 ± 36	−125 ± 15	−7 ± 36	0.5 ± 0.1	0.2
Magnetite	426 ± 184	−23 ± 6	81 ± 16	57 ± 10	47 ± 4	32 ± 10	0.9 ± 0.3	3.6
C-rich	570 ± 125			13 ± 6	8 ± 2	8 ± 6	0.5 ± 0.1	16.8
δD hotspot	7012 ± 792						0.4 ± 0.1	0.4
δD hotspot	4494 ± 722						0.4 ± 0.1	0.3
Amberley3								
Bulk	52 ± 79	−29 ± 1	275 ± 5	−1 ± 5	−2 ± 2	0 ± 5	1.6 ± 0.5	76.8
C-poor	−166 ± 76	−28 ± 6	364 ± 17	−4 ± 6	3 ± 2	−6 ± 6	4.6 ± 1.4	14.2
C-rich	459 ± 130	−38 ± 3	266 ± 10	5 ± 10	0 ± 4	5 ± 10	0.8 ± 0.2	4.7
D-rich	1610 ± 268	−94 ± 5	310 ± 24	−3 ± 17	−9 ± 7	2 ± 18	0.8 ± 0.3	1.0
$\delta^{17}O$ hotspot	−384 ± 438	−154 ± 86	682 ± 308	365 ± 55	−56 ± 20	394 ± 56	9.3 ± 2.9	0.1
Meteoritic IOM[b]								
CV3 oxA								
Allende	194 ± 13	−17.0 ± 0.2	−51.2 ± 0.6		5.1 ± 0.4		0.2	
CV3 oxB								
Kaba	209	−15.4	−26.2		17.8		0.3	
CM2								
Murchison	777 ± 27	−18.9 ± 0.0	−1.0 ± 0.4		13.2 ± 0.6		0.6	
CM2								
Bells	3283	−34.2 ± 0.2	415.3 ± 1.6		14.1 ± 0.2		0.7	
LL3.2								
Krymka	1917	−17.4	−10.7		12.2 ± 0.4		0.3	
L3.05								
QUE 97008	3199	−20.4 ± 0.1	−0.7 ± 0.1		8.4		0.4 ± 0.1	
CR2								
GRA 95229	2909	−21.6 ± 0.9	153.4 ± 6.7		12.1		0.7	
CR2-an								

Table 3. *Continued*. Carbon, hydrogen, nitrogen, and oxygen isotope results for IDPs in this study.[a]

Samples	Isotopic compositions (‰)						H/C[d]	ROI area (μm^2)
	δD	$\delta^{13}C$	$\delta^{15}N$	$\delta^{17}O$	$\delta^{18}O$	$\Delta^{17}O$[c]		
Al Rais	2619	−24.2	161.8		15.2		0.8	
Terrestrial material								
1-HOBt	−34.5	−28.7	0.4					
San Carlos olivine				2.6	4.9	0.1		

[a]Errors are reported as two standard deviations of the mean of multiple analyses (all image planes combined for each analysis; 2σ), which have taken into consideration the error based on counting statistics, the IMF, as well as the reproducibility of standards measured during the different analytical sessions over the course of this study. The IMF factors of H, C, N, and O isotopic analyses, based on analyses of the 1-HOBt and San Carlos olivine standards, are 0.921 ± 0.067 (2σ), 1.006 ± 0.001, 1.023 ± 0.002, and 0.986 ± 0.004, respectively.
[b]Data are from Alexander et al. (2007).
[c]$\Delta^{17}O = \delta^{18}O - 0.52 \times \delta^{18}O$; $\sigma\Delta^{17}O = \sqrt{\sigma^{17}O^2 + 0.2704 \times \sigma^{18}O^2}$.
[d]$H/C = H^-/^{12}C^-$.

Different individual particles belonging to the large Drake cluster have been characterized by earlier studies (Floss et al. 2010; Davidson et al. 2012; Starkey and Franchi 2013). The presence of presolar grains, highly disordered OM, N anomalies, and the enrichment in D suggest a cometary origin for Drake (Davidson et al. 2012). Davidson et al. (2012) suggested that Drake is possibly derived from comet Grigg–Skjellerup, which supports the view that several particles from the GSC are indeed fresh from this comet (Busemann et al. 2009). Comet Grigg–Skjellerup has close encounters with the Earth in April each year with peak fluxes in 2003 and 2004, which led to the prediction by Messenger (2002) that 1–50% of the background interplanetary dust flux in the >40 μm size was dust from this comet. The presence of high-Ni Fe-sulfides ($Fe_{0.6}Ni_{0.7}S$ pentlandite) in Drake3 might seem contradictory to the anhydrous/cometary origin, as they are abundant in hydrated IDPs, and had previously been used as an indicator of parent body aqueous processing (Zolensky and Thomas 1995). Nevertheless, their association with abundant GEMS (which are rapidly hydrated on exposure to water; Nakamura-Messenger et al. 2011) in CP-IDPs suggests that they were not produced by aqueous processing after assembly of the dust particles and incorporation into a parent body (Flynn et al. 2016), and can be formed at or upon cooling from high temperature (Schrader et al. 2016).

Three presolar silicate grains were located in Drake4, and two C, N anomalous hotspots in Drake3 (Table 3 and Fig. 8). O and N hotspots have also been observed for another IDP grain the same Drake cluster (L2055 Cluster 5), with a presolar silicate abundance of 920 ± 700 ppm (Davidson et al. 2012). On the contrary, the apparent absence of presolar grains and C, N isotopic anomalies in the particle (L2055-B3) from the Drake cluster studied by Floss et al. (2010) led the authors to believe that Drake is less primitive. The disparity in the isotopic compositions of different particles within the same IDP cluster testifies for a significant spatial heterogeneity in the mix of presolar grains and primitive materials among IDPs. The spatial N heterogeneity likely reflects that the macromolecular carbon in the Drake cluster contains both ^{15}N-rich and ^{15}N-poor carriers of different origins. Drake3 has possibly incorporated a larger proportion of ^{15}N-enriched N-containing organic hosts, which was synthesized prior to the aggregation of the cluster, and therefore, the same level of ^{15}N-enrichment is not seen in Drake4. The disparity between the presence of isotopic hotspots in various Drake particles led Davidson et al. (2012) to a conclusion that the use of the presence/abundances of presolar grains/isotope anomaly hotspots alone is not sufficient to determine the "primitiveness" of an IDP cluster. The key question associated with such heterogeneity is how and when the primitive materials were mixed with the less primitive materials.

O and H isotopic anomalies have also been observed in Balmoral3b (Table 3; Figs. 8 and 10). The three presolar silicate grains in Balmoral3b belong to group 1 and 3 presolar grains (Nittler et al. 1997; Boothroyd and Sackmann 1999). Another particle from the Balmoral cluster (L2071 Cluster 2) was studied previously and found to contain rare, very ^{16}O-depleted regions ($\delta^{17}O$, $\delta^{18}O$ = +80‰ to +200‰; Starkey et al. 2014). The ^{16}O-depleted components of Balmoral were suggested to have formed in an extremely ^{16}O-depleted reservoir that originated from oxygen isotope self-shielding of CO, in the comet-forming regions at large heliocentric distance (i.e., the outer solar nebula/ISM; Starkey et al. 2014). The fact that particle Balmoral3b in this study contains a wide mixture of primitive (e.g., presolar silicates, Fig. 8) and less primitive components (e.g., moderately ordered OM, Fig. 4), and the presence of both ^{16}O enriched and depleted O anomalies, marries well with the hypothesis that the original bodies of

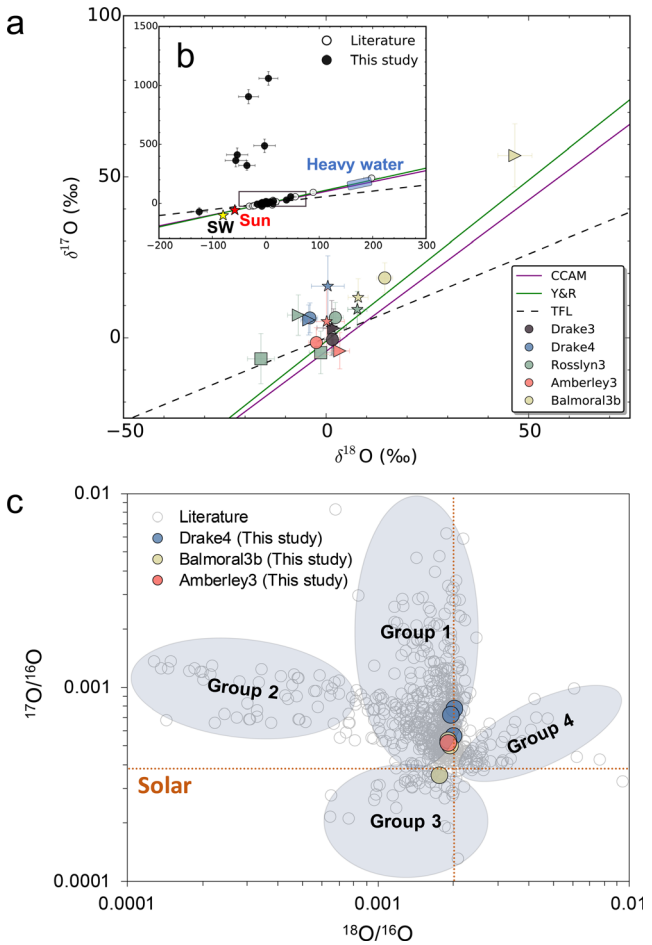

Fig. 8. a) O three-isotope plot comparing the bulk oxygen isotopic compositions of the IDP samples to that of other solar system materials. The isotopic compositions of the sample bulk are shown as ●, C-rich areas as ★, C-poor areas as ▶, and Fe-rich areas as ■. b) Anomalous presolar grain data on a larger scale. CCAM, carbonaceous chondrite anhydrous mineral (slope = 0.94), represents the primitive oxygen isotope reservoir of the early solar nebula, based on analyses of anhydrous minerals from calcium-aluminum-rich inclusion (CAI) in Allende (Clayton and Mayeda 1999); Y&R, Young and Russell (slope = 1), defined based on measurements made on (aqueous) alteration-free areas of CAI in Allende (Young and Russell 1998); TFL, terrestrial fractionation line (slope = 0.52), which passes through the origin defined by standard mean ocean water (SMOW), is representative of the terrestrial planets and related differentiated bodies of the inner solar system (Matsuhisa et al. 1979). O compositions of major primary components solar wind (SW) and the Sun are from McKeegan et al. (2011). c) O three-isotope plot of O-anomalous presolar grains from IDPs from this study (filled circles) and the literature (open circles). IDP data are from Floss et al. (2006) and references therein. Error bars of data in this study are smaller than the symbols. The four O isotope groups established by Nittler et al. (1997) for presolar oxide grains are indicated by the shaded areas. Orange dotted lines indicate the solar O isotopic ratios.

Balmoral could have been disrupted through collisional events, and then re-incorporated into new "brecciated" bodies (Starkey et al. 2014).

Rosslyn belongs to a very large IDP L2036 Cluster 4 and particles from this cluster had been widely studied in the past (e.g., Aléon et al. 2006; Messenger et al. 2007, 2009, 2010; Busemann et al. 2011; Nakamura-Messenger et al. 2012). Rosslyn contains GEMS grains and a minor development of magnetite (Messenger et al. 2007, 2009, 2010), suggesting only a moderate extent of atmospheric entry heating. However, Rosslyn has been described to contain a high abundance of presolar silicate grains (~2000 ppm) hosted within an unusually high abundance of an assemblage of polycrystalline grains, or equilibrated aggregates, which suggests that these grains had experienced a thermal annealing process that potentially occurred in the solar nebula (Messenger et al. 2007, 2009). The H/C ratios and isotopic compositions of Rosslyn3 and Amberley3 are similar and they are plotted in roughly the same region as opposed to the type I IDPs, which suggest that the OM in Rosslyn3 and Amberley3 shares a similar origin and/or has experienced a similar processing history. Amberley3 contains sulfide–silicate intergrowths which have been observed in the comet 81P/Wild 2 samples and CP-IDPs that belong to large clusters, while the sulfide–silicate intergrowths were believed to have formed by thermal metamorphic processes in the nebula (Joswiak et al. 2009).

OM in IDPs Is Structurally Distinct from Chondritic OM

Raman spectra of poorly ordered materials like the macromolecular materials in carbonaceous chondrites are correlated with the nature of the organic precursors and the structural order of the aromatic units (Wopenka and Pasteris 1993; Quirico et al. 2009). Therefore, variations in the Raman peak parameters can indicate the presence of different chemical components, relative OM maturity, and different alteration history (e.g., temperature, duration of the heating event).

Previous Raman analyses of IDPs suggest that the Raman signatures of IDP IOM are similar to IOM in CM and CR chondrites (e.g., Quirico et al. 2005; Muñoz Caro et al. 2006; Busemann et al. 2009; Brunetto et al. 2011; Starkey et al. 2013). The Raman signatures of IDP OM in this study also show affinities to highly disordered organics in primitive chondrites that are composed of polyaromatic or amorphous OM with conjugated bonds. Increasing metamorphism results in the transition from amorphous to graphitic carbon, leading to a narrower Γ_D and larger I_D/I_G observed for the thermally

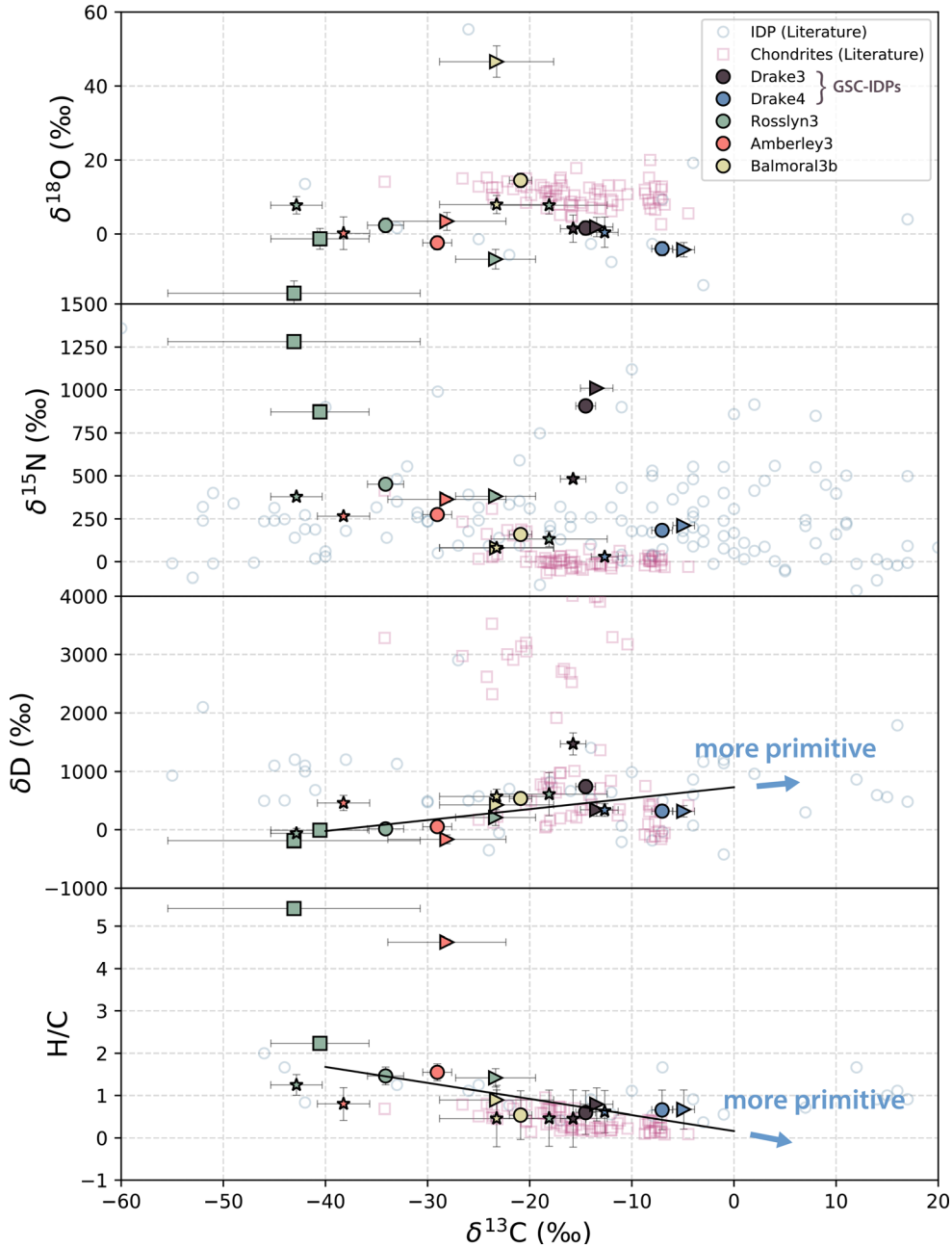

Fig. 9. Comparison of the $\delta^{13}C$ values to the $\delta^{18}O$, $\delta^{15}N$, δD values and H/C ratios of the IDP samples. The isotopic compositions of the sample bulk are shown as ●, C-rich areas as ★, C-poor areas as ▶, and Fe-rich areas as ■. Trend lines are calculated from bulk isotopic data of the five IDPs in this study. Literature data of chondritic IOM and bulk IDPs are shown as open □ and ○ symbols, respectively (Messenger 2000; Floss et al. 2006; Alexander et al. 2007; Busemann et al. 2009; Davidson et al. 2012; Matrajt et al. 2012; Starkey and Franchi 2013; Starkey et al. 2014).

metamorphosed meteorites (e.g., Ferrari and Robertson 2000; Busemann et al. 2007), and the Raman D parameters of IDP OM follow such trend (Figs. 4a and 4b). CP-IDPs are thought to represent the most primitive solar system object that have only experienced no/minimal thermal metamorphism (e.g., Messenger 2000; Quirico et al. 2005; Floss et al. 2006; Starkey et al. 2013); therefore, their OM is certainly not fully graphitized, albeit heated to varying extents during atmospheric entry (e.g., Sandford and Bradley 1989; Germani et al. 1990; Flynn et al. 1992; Keller et al. 1992, 2004; Greshake et al. 1998; Rietmeijer 2004; Matrajt et al. 2006).

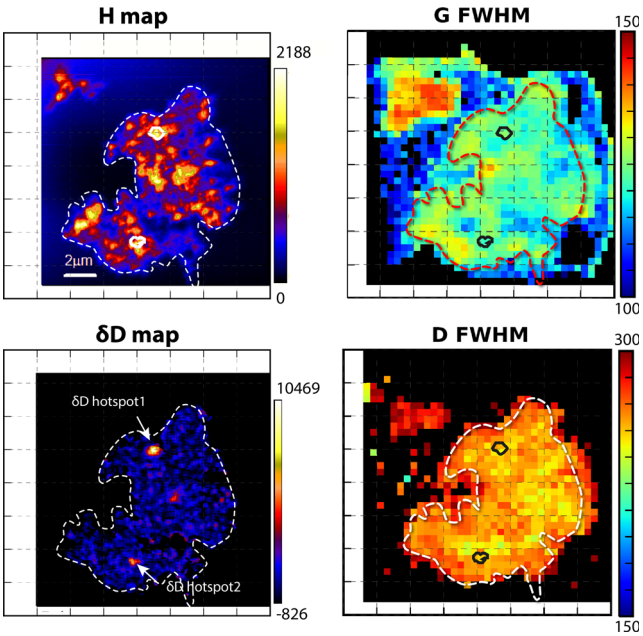

Fig. 10. NanoSIMS elemental (H), δD isotopic, and the Γ_D, Γ_G maps of Balmoral3b. Locations of the two δD hotspots are shown on the maps, which indicate that the isotopic anomaly is not associated with any Raman C anomalies. Raman maps (pixel size: 0.5 × 0.5 mm^2).

Although IDP OM has affinities to that of primitive chondrites, a detailed comparison between the Raman band parameters of the OMs reveals that the two are distinct from each other. IDP OM generally has wider band widths (Γ_D, Γ_G), lower I_D/I_G ratios, and higher D band positions (ω_D) than that in less primitive (more thermally altered) meteorites (Fig. 4). The maturity trend and the Γ_G values of the IDP OM clearly deviate from those of the chondritic OM (Figs. 4c and 4d). This disparity between the Γ_G values of the chondritic and IDP OM has been noted in the past (Raynal et al. 2001; Quirico et al. 2005; Busemann et al. 2009; Brunetto et al. 2011; Starkey et al. 2013), which was suggested to reflect the presence of a different class of carbonaceous material in IDPs when compared to other extraterrestrial material (Raynal et al. 2001; Quirico et al. 2005), and that IDPs contain more disordered organic carbon than chondritic meteorites (Busemann et al. 2009; Starkey et al. 2013).

In order to elucidate the disparity in the Raman band parameters of IDP and chondritic meteorite OM, it is imperative to appropriately correlate the Raman spectral parameters to the nature of the carbon bonds and molecular morphology. In graphitic materials, the two E_{2g} double degenerate in-plane vibration modes of the D^4_{6h} space group symmetry are Raman active (Tuinstra and Koenig 1970; Wang et al. 1990; Ferrari and Robertson 2000; Sadezky et al. 2005). The second mode, E_{2g2} mode, corresponds to the C–C stretching vibration that contributes to the G band; thus, a perfectly stacked graphite has a sharp narrow G band that corresponds to the sp^2 carbons of the graphene network, and the nonbonding π-orbitals only give rise to weak Van der Waals forces with minimal influences to the parallel carbon layers. The 1580–1600 cm^{-1} region is often characterized as a single asymmetric composite G_L band (Ferrari and Robertson 2000; Lahfid et al. 2010; Kouketsu et al. 2014). In poorly ordered material, the G_L band is comprised of both the G band and a component of the D band (the "D2 band" at ~1620 cm^{-1}). This composite G_L band becomes too broad to be properly decomposed separately into the D and G bands. In such circumstance, the G band is not solely correlated to graphitic materials, and therefore, it is difficult to pinpoint the variation in the G_L band peak parameters to a particular factor. In contrast, the ~1350 cm^{-1} D1 band is attributed to the A_{1g} mode, which is inherent in the graphite lattice and becomes observable when symmetry is broken by an edge (i.e., in-plane defects), and is not present in perfectly stacked graphite. Therefore, while the D band parameters are strong tracers of the maturity of OM that are directly correlated with the presence of defects, the G band is influenced by the composition of individual aromatic units, the size of the in-plane sp^2 domains, and the entire structure of the carbon network. As such, Γ_G and OM maturity are not always correlated and the G band does not simply trace the thermal metamorphism grade.

The D band parameters indicate that the OM in IDPs and primitive chondrites share similar OM maturity (Fig. 4a), and the disparity observed for their G band parameters indicates the presence of different non-aromatic organic components (Fig. 4d). Different types of organic precursors should mature in a distinctive manner (Wopenka and Pasteris 1993); therefore, the observed deviation in the trend of the G band parameters suggests that the organics in IDPs and meteorites are structurally different, and/or they gained maturity in a different manner. As the G band occurs in sp^2 paired carbon atoms (all sp^2 sites, not only in rings), the disparity in G parameters but similarity in D band parameters of IDP and chondritic OM suggests that their sp^2 olefinic contents are different. This hypothesis marries well with previous reports of (1) the absence of Raman D band (aromatics) but the presence of G band (olefins) in IDPs with a possible cometary origin (Muñoz Caro et al. 2012), (2) the presence of a strong absorption feature at ~285 eV (1s–π* transition in aromatic or olefinic carbon, i.e., PAHs or olefins) but the absence of the ~290 eV feature (1s–σ* exciton peak

in graphene) in C- X-ray absorption near-edge structure (XANES) spectra of IDPs (Flynn et al. 2003). Although the ~285 eV feature of IDP OM is commonly interpreted as the presence of PAHs (Flynn et al. 2003, 2004; Keller et al. 2004), some contribution from olefins cannot be ruled out.

The Raman band parameters of the IDP OM are comparable to that of the experimentally heated (short-term heating) Tagish Lake meteorite reported in Chan et al. (2019; Fig. 6). While the D band parameters follow the maturity trend exhibited by chondritic OM in both the IDP and Tagish Lake OM (Fig. 6a), the disparity (widening) of the Γ_G value in IDP OM versus chondritic OM is well demonstrated by the experimentally heated Tagish Lake samples (Fig. 6b). The observed Γ_G widening indicates the development of crystalline domains without graphitic ordering, as large-scale graphitization would have reduced the Γ_G value (Chan et al. 2019). This interpretation is consistent with an absence of the graphene structure (~291.6 eV) in the C-XANES spectrum of the experimentally heated Tagish Lake that corresponds to a 1s–σ* exciton, which develops when highly conjugated sp^2 bonded C domains were present, as in the long-term thermally metamorphosed type 3 chondrites (Cody et al. 2008). Without extensive graphitization, short-term heating of Tagish Lake meteorite may have led to the increase in the abundances of carboxyl moieties by processes such as carboxylation (Gaydou et al. 2017; Juliá-Hernández et al. 2017; Yang and Lee 2019) with the C and O contributed by the decompositions of carbonate and the CO (and/or CH_n) moieties. Therefore, the comparable Raman band parameters between experimentally heated Tagish Lake meteorite and the IDP samples could indicate that IDP OM has been exposed to short-term heating, or a unique IDP organic structure that is different from chondritic OM, with a higher abundance in non-aromatic sp^2 contents and heteroatoms (e.g., oxygenated-moieties) as bridging material.

Contamination from silicone oil that was used to capture the IDP grain on the flat plate collection surfaces is probably not the culprit for the observed OM nature, because silicone oil has a very characteristic Raman spectrum that can be easily distinguished if it were present. Silicone oil has two sharp bands in the range of 1200–1000 cm^{-1} that are assigned to the Si–O–C and to the Si–O–Si stretching vibrations, and a band at 1600–1300 cm^{-1} that can be assigned to the bending vibration bands of CH_x aliphatic groups (Österle et al. 2015). These bands are clearly absent from the Raman spectra of the IDP samples.

The process that best describes such variation in the nature of the IDP and chondritic OM is perhaps the disordering of carbon from nanocrystalline graphite in chondritic IOM to low sp^3 hydrogenated amorphous carbon in IDP IOM likely induced by amorphization due to exposure to irradiation in space. Amorphization of OM could be achieved via processes such as irradiation by low energy solar wind ions (Brunetto et al. 2009, 2015; Lantz et al. 2017), cosmic rays, and ultraviolet photons during their residence in the ISM and/or outer regions of the protoplanetary disk (Ferrari and Robertson 2000; Strazzulla et al. 2001; Muñoz Caro et al. 2006). Previous irradiation experiments on extraterrestrial organics and their analogs have shown that ion irradiation can induce amorphization of carbonaceous material, in particular the Γ_G value was reported to increase significantly (Baratta et al. 2004, 2008; Brunetto et al. 2009). Amorphization can break sp^2 (graphite-like) bonds and eventually lead to the formation of amorphous carbon (a-C) and the hydrogenated analog hydrogenated-amorphous carbon (a-C:H) with high sp^3 (diamond-like bond) contents (maximum 20% C–C sp^3 and 20 at% of H content in a-C; 40–60% C–C sp^3 and 30–50 at% of H content in a-C:H; Robertson 2002; Casiraghi et al. 2005). Most sp^3 sites are bonded to hydrogen or heteroatoms, where the sp^2 sites can still exist as rings as well as chains, and the molecular morphology is typically associated with increasing H content and reducing sp^2 cluster/domain sizes. The aliphatic CH_2/CH_3 ratios of CP-IDPs are typically two times higher than meteoritic IOM (Flynn et al. 2003; Brunetto et al. 2011; Alexander et al. 2017).

Busemann et al. (2007) observed a correlation between the Γ_G value and H/C ratio in meteoritic IOM. Therefore, a wider Γ_G suggests potentially larger H/C ratio in the IDPs compared to the meteoritic IOM (Keller et al. 2004; Muñoz Caro et al. 2006). IDP OM is more disordered than the meteorite IOM, highly enriched in H, and the high H/C ratios are also observed for the five IDPs in this study (Fig. 9). The structure of IDP OM would be more comparable to the terrestrial type I kerogen (H/C = 1.29; O/C = 0.06), whereas chondritic OM would be comparable to type II kerogen which contains mature organics with a high level of carbon condensation (H/C = 0.57; O/C = 0.06; Weck et al. 2017; Fig. 11). The high H/C ratios of IDP OM suggests that they were formed and subsequently resided at low temperatures to allow the preservation of these elemental ratios (Pizzarello et al. 2006).

Effects of Atmospheric Entry Heating on the IDP Organics

CP-IDPs are typically more C-rich than chondrite matrix (Schramm et al. 1989), and the main H and N carrier is the OM (Alexander et al. 2017), which comprises molecules with functional groups such as

carbonyl (C=O; Flynn et al. 2003), methyl ($-CH_3$), methylene ($=CH_2$; Brunetto et al. 2011), and amine ($-NH_2$; Clemett et al. 1993). The organic and isotopic compositions of IDP and meteoritic OM are heterogeneous at the (sub-) μm-scale (Aléon et al. 2001; Busemann et al. 2009); however, it is unclear how atmospheric entry heating (short-term heating at pyrolysis temperatures) influences the OM components, the associated Raman spectra, and the intraparticle OM isotopic heterogeneity.

As IDPs were frictionally heated during atmospheric entry, it can be inferred from the mass of the object the extent of heating it has experienced (i.e., smaller/more porous/lighter particles are the less heated IDPs). In light of the high internal porosities and anhydrous mineralogy of cometary IDPs, they were suggested to have a much lower average density than asteroidal IDPs (cometary IDPs: 1.0 g cm^{-3}; asteroidal IDPs: 3.3 g cm^{-3}; Joswiak et al. 2007). Despite the lower average density, cometary IDPs were estimated to have experienced higher atmospheric entry temperatures than asteroidal IDPs (Flynn 1989; Sandford and Bradley 1989; Love and Brownlee 1991). This reflects that factors such as eccentricity and inclination, which influence the entry angle, and speed, can also affect the degree of atmospheric entry heating. As most individual IDPs are between 5 and 15 μm in diameter (Flynn 1989; Bradley 2003), they can survive the heating without being completely vaporized on atmospheric entry. Cometary IDPs of smaller particle sizes (<10 μm) that were derived from comets with perihelia >1.2 astronomical units (AU) were not heated to temperatures above 600 °C during atmospheric entry (Flynn 1989; Sandford and Bradley 1989). Therefore, although comet 26P/Grigg–Skjellerup (perihelion = 1.1 AU, eccentricity = 0.66, atmospheric entry velocity = 22 km s^{-1}) has a perihelion of just under the 1.2 AU benchmark, it has a sufficiently low eccentricity to deliver to the Earth dust particles at low atmospheric entry velocities/heating.

Most of the giant particle clusters (10–20% of collected stratospheric IDPs) are CP-IDPs, some of which are thought to have a cometary origin (Bradley 2003). With higher eccentricity, inclination, and atmospheric entry velocity, large cometary IDPs are more significantly heated during atmospheric entry (Flynn 1989; Sandford and Bradley 1989; Jackson and Zook 1992; Brownlee et al. 1995). For example, with a perihelion of 0.6 AU, dusts from 1P/Halley comet could have experienced atmospheric entry velocities as high as 65 km s^{-1} (Flynn 1989). Cometary particles of >20 μm in size with perihelia <1.2 AU can be heated to more than 900 °C at full depth. The elevated temperatures experienced by larger IDPs with smaller perihelia typically lasted for several seconds during their atmospheric entry (Flynn 1989; Sandford and Bradley 1989; Love and Brownlee 1991), which could have thermally decomposed any organics present, regardless of the kinetic effects (i.e., short heating duration cannot enhance OM survival; Matrajt et al. 2005). Heating at these temperatures could result in annealing (erasure) of the solar flare tracks (Fraundorf et al. 1982; Sandford and Bradley 1989), He and/or volatile depletion (He is lost at 600–1200 °C; e.g., Flynn et al. 1992; Brownlee et al. 1995), the development of magnetite rims (Germani et al. 1990; Flynn et al. 1992; Keller et al. 1992), and mineralogical transformation from hydrous minerals into anhydrous components (Greshake et al. 1998).

The data in this study demonstrate a correlation between the elemental, chemical, and isotopic compositions of the IDP samples, which could provide some insights into the extent of heating an IDP has experienced. In general, the less heated type I IDPs contain a larger proportion of pristine OM with higher heteroatoms abundances reflected by the strong fluorescence signature (Fig. 3a), higher δD and $\delta^{13}C$ values, but lower H/C ratios (Fig. 9) and smaller crystalline domains (aromatic units; Fig. 4a). The alterations in the isotopic values are not ideal, as they would have masked the intrinsic isotopic signature of the indigenous OM. This would have modified the δD and $\delta^{13}C$ values of the IDP OM from extraterrestrial to terrestrial values (Fig. 12), which compromise the study of IDP OM on ground of their "primitive" nature. The $\delta^{15}N$ values appear less influenced by the heating effect, which indicates that the OM exhibits a significant N heterogeneity (localized N isotopic anomalies such as isotopically heavy organic nanoglobules (Matrajt et al. 2012; Messenger et al. 2008; Nakamura-Messenger et al. 2006), or the presence of refractory ^{15}N-containing organic hosts. The observed reduction in the bulk $\delta^{13}C$ is also supported by the experimental heating of the Murchison meteorite, which shows that the bulk $\delta^{13}C$ is reduced by 2.3‰ from −17.9 to −20.2‰ when Murchison was heated from 600 to 900 °C for 50 h (T. Nakamura, personal communication). On a shorter timescale, meteorites that were suggested to have experienced short-term (impact) heating also show a trend of decrease in δD with impact heating (Yabuta et al. 2010).

The OM in Drake3 and Drake4 is among the most disordered of all IDP OM studied by far (Fig. 5). The C-rich region of the GSC-IDP Drake3 (Figs. 2 and 7) contains the most pristine OM among the five IDP samples. A small degree of correlation was observed for the Raman G band parameters of Drake3 ($R^2 = 0.57$) (Fig. S2), in a way similar to the correlation observed

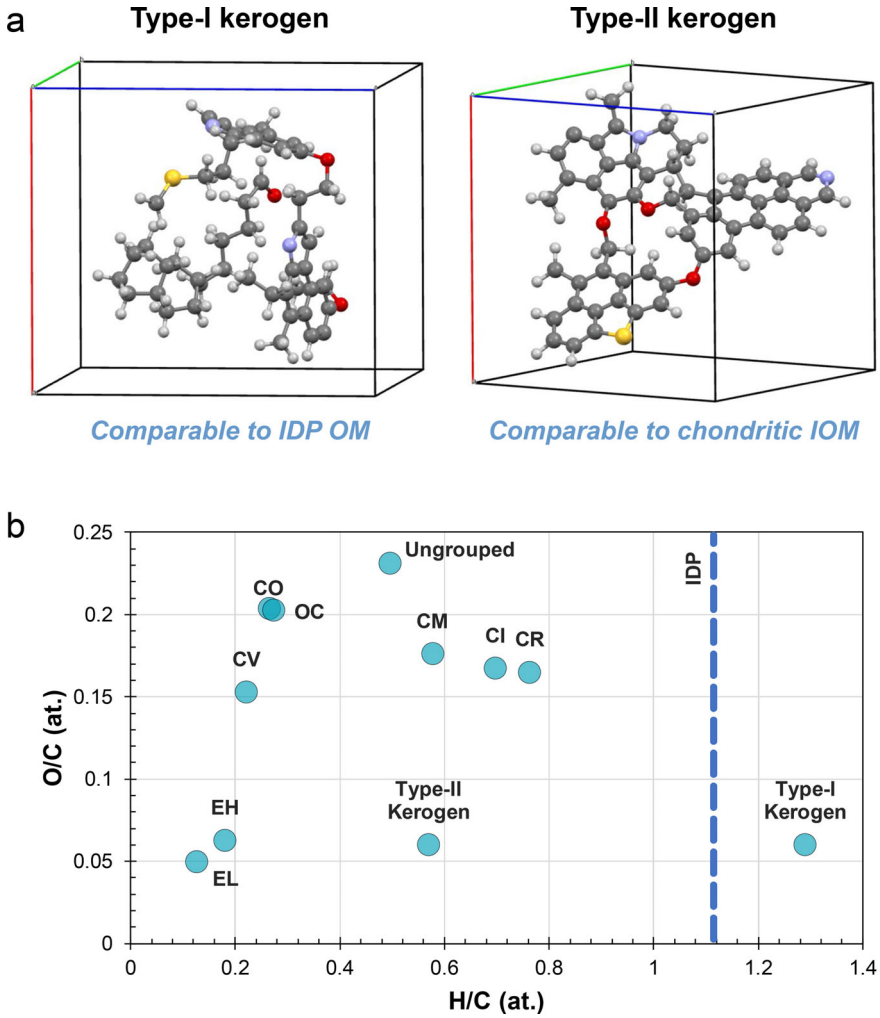

Fig. 11. a) Structures of type I (left) and type II (right) kerogen models from Weck et al. (2017), which are suggested in this work to be comparable to IDP OM and chondritic IOM, respectively. The various types of kerogen are used to describe the maturity level and the type of organics present (Ungerer et al. 2015). Type I kerogen (H/C = 1.29; O/C = 0.06) is composed predominantly of long alkyl chains linked with saturated and aromatic cyclic structures. Type II kerogen has a lower hydrogen content (H/C = 0.57; O/C = 0.06) and thus has a higher maturity level (Weck et al. 2017). Color legend: gray, C; white, H; purple, N; red, O; yellow, S. b) Comparison of the H/C and O/C ratios between IDP OM, chondritic IOM, and types I and II kerogen. Primitive CM, Ivuna-like (CI), and CR meteorites share similar H/C and O/C ratios and their H/C ratios are comparable to type II kerogen. With a H/C ratio of 1.1, IDP OM is distinctive from chondritic IOM, and is more comparable to the immature type I kerogen. The average H/C ratio of IDP OM is obtained from this study and data from the literature (Davidson et al. 2012; Starkey and Franchi 2013; Starkey et al. 2014) and the H/C and O/C ratios chondritic IOM are from Alexander et al. (2007). The propagated errors are for both H/C and O/C values of chondritic IOM are all below 0.03.

for the G band parameters in meteoritic IOM, suggesting OM micrographitization described in Busemann et al. (2007). The intraparticle dispersion of Raman band parameters reflects the presence of primitive carbon unaltered by annealing processes, which would otherwise have erased the signature of heterogeneity in OM maturity.

Drake OM is D- and ^{13}C-enriched and contains a higher proportion of sp^3 to sp^2 contents (IDPs could have sp^3 content as high as 30%; Muñoz Caro et al. 2006). It could represent the most pristine OM formed by low-temperature H-fractionating chemistry in the outer disk (Terzieva and Herbst 2000). Ion molecule reactions in ISM molecular clouds that involve the irradiation of organic precursors and ices containing D- and ^{15}N-enriched gas phase precursor molecules such as H_2O, CH_3OH, and NH_3 can also produce a complex network of organic molecules (e.g., a-C:H, amino acids and N-heterocycles such as nucleobases (e.g., Dartois et al. 2005) that are often D- and ^{15}N-enriched (e.g.,

$\delta D_{amino\ acids}$ = +868 to +7245‰ and $\delta^{15}N_{amino\ acids}$ = +77 to +139‰; Pizzarello and Holmes 2009). Prolonged ion irradiation of the carbonaceous material can ultimately lead to the amorphization via the breaking of sp^2 bonds and the formation of a-C (Dartois et al. 2005; Muñoz Caro et al. 2006; Busemann et al. 2007).

Amberley3 (L2076 Cluster 7) represents the most heated IDP sample analyzed in this study with Raman band parameters dissimilar to primitive meteorites, but closer to the OM of the moderately heated OC (between Queen Alexandra Range [QUE] 97008 with a peak metamorphic temperature [PMT] of 250 °C and Krymka with a PMT of 290 °C; Busemann et al. 2007, fig. 4). The I_D/I_G ratio of the Amberley3 OM is higher than that of primitive meteorites, which suggests that the OM has been processed by thermal annealing, via the loss of hydrogen and heteroatoms and the formation of polyaromatic structures. Nevertheless, the I_D/I_G ratio and Γ_D value would have been greatly reduced if the OM has experienced large-scale graphitization (Ferrari and Robertson 2000) to the extent undertaken by the most metamorphosed meteorites (e.g., Ornans-like [CO] 3.7 Isna and CV3 Meteorite Hills [MET] 01017, see fig. 6 in Busemann et al. 2007). As the I_D/I_G ratio and Γ_D value of Amberley3 OM are both significantly higher than that of the metamorphosed Allende OM (Fig. 4b), it suggests that the graphitization process in Amberley3 has not been completed, or that the OM precursor of Amberley3 is more enriched in heteroatoms (e.g., oxygenated-moieties) as bridging material. If Amberley3 was exposed to short-term heating that did not lead to complete graphitization of the OM, Amberley3 OM would be more comparable to the Tagish Lake meteorite OM experimentally heated to 600–900 °C (Fig. 6). The bulk isotopic composition of Amberley3 is notably depleted in D but not ^{15}N. Enrichment in ^{15}N and depletion in D have been observed in thermally processed IDPs in the past (Keller et al. 2004), which suggest the loss of a labile D-host via flash heating, while the ^{15}N-host is resilient to heating and D-depleted.

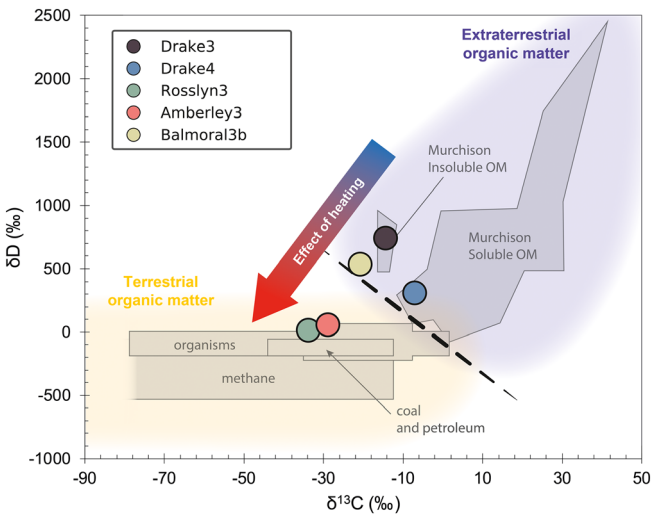

Fig. 12. Comparison of the δD and $\delta^{13}C$ values of terrestrial and extraterrestrial OM. Isotopic data of terrestrial OM and Murchison soluble and insoluble OM are obtained from Butterworth et al. (2004), Sephton and Botta (2005), and references therein.

Thermal annealing typically enhances aromaticity by converting the aliphatic sp^3 C into aromatic sp^2 C, leading to an increase in the size of the aromatic moieties and a reduction in the overall H/C ratio (Dischler et al. 1983; Derenne and Robert 2010; Jones 2012). This trend is observed for chondritic OM (e.g., Alexander et al. 2007; Busemann et al. 2007). Chondritic IOM has a significant proportion of amorphous carbon with sp^2 bonded C components but rather a smaller sp^3 C–C content; therefore, heating of chondritic IOM decreases the aliphatic components and the H/C ratio, while keeping the C abundance unchanged (Alexander et al. 2014). However, our Raman and NanoSIMS observations suggest the opposite for the IDP OM. IDP OM that has been less heated (i.e., more primitive, based on the Raman D parameters—higher Γ_D and ω_D values; Fig. 4a) has lower H/C ratios (Fig. 9; e.g., $\Gamma_{D\ (Drake3)}$ = 260.8 ± 16.2 cm^{-1}, $\Gamma_{D\ (Amberley3)}$ = 207.9 ± 12.9 cm^{-1}, $H/C_{(Drake3)}$ = 0.6; $H/C_{(Amberley3)}$ = 1.6; Tables 2 and 3). The results are unexpected, and a possible explanation for this is the presence of a significant proportion of disordered C with low H content, such as a-C:H with a high sp^3 C–C contents, carbonyl (C=O), or alkene (olefin C=C) groups as bridging material occurring between the sp^2 aromatic sites. Decomposition of these low H materials, such as by decarboxylation of the carboxyl content and losing the C as CO_2, leads to a higher overall H/C ratio.

Porous media can offer a heat shield effect to the OM. Pulse-heating experiments (5 s) of IDPs that covered a temperature range of 700–900 °C indicated that a few percent of organic molecules (e.g., PAH, ketone, amino acids) adsorbed in a microporous medium could survive the heating (Matrajt et al. 2006). This is supported by the presence of OM in the fine-grained areas in IDPs in this study (Fig. 2). Also, both SEM-EDX and Raman analyses indicate that C-rich components are more common in the fine-grained matrices of the IDPs as compared to those that are associated with larger mineral phases like sulfides, metals, and forsterite (Fig. 2). The Raman band

parameters indicate that the OM contained within different IDP components are structurally different. Fine-grained, C-rich areas are often associated with the regions with high Γ_G values and low Γ_D in the Raman maps (Fig. 2), suggesting that they are dominated by highly disordered amorphous C with high aliphatic/aromatic ratios and heteroatom abundances. Atmospheric entry heating induces a twofold heating effect on the IDP IOM (Fig. 13). The unshielded OM associated with mineral phases is subjected to full-scale adiabatic heating. Thermal decomposition of hydrocarbon via cracking (i.e., breaking of C–C bonds) results in a low OM abundance indicated by the generally lower Raman intensities (Fig. 3a, points C–G). Laser focus could arbitrarily influence the Raman intensities—Raman signal intensity can be reduced if the laser is not well focused at the sample surface. However, it would be more difficult to obtain a good focus on fine-grained materials than the flat large mineral grain surfaces. Therefore, the lower Raman signal intensity detected on large mineral grain surfaces than fine-grained material does not simply reflect poor laser focus. Cracking also leads to fragmentation of large IOM structure into light hydrocarbons, and thus, the heated phases are associated with disordered OM with wide Γ_D values (Fig. 2, Amberley3). In contrast, OM in the fine-grained matrix can survive full-scale thermal decomposition, although high-temperature annealing can cause clustering of the sp^2 sites into ordered aromatic rings and maturity in the OM structure in a way similar to thermal metamorphism. The IDPs in this study are fragments from large cluster particles which were fragmented into smaller pieces on contact with the collector. The temperature gradients of larger particles account for a hot ablating surface and a relatively cool interior, and thus, the positions of IDPs in larger clusters and the density of the cluster particle could also have influenced the extent of the heating. This should be further investigated in future studies.

Nevertheless, as the annealing process has altered the OM irreversibly, simply by referring to the OM structure, it is difficult to pinpoint the heat source, or to elucidate when the heating took place. The heating regime could have occurred any time since the formation of the OM, such as by transient heating induced by impact and/or solar radiation (Nakamura 2005; Wooden et al. 2007), and/or atmospheric entry heating. Thermal metamorphism in the solar nebula has been proposed to account for the occurrence of high-temperature objects (e.g., GEMS, sulfide–silicate intergrowth) in some IDPs and samples returned from the Wild 2 comet (Joswiak et al. 2009, 2017; Keller and Messenger 2011). Sulfide–silicate intergrowths which formed at high temperatures have been observed for Amberley3 in this study (Fig. 2). However, the presence of these high-temperature phases alongside OM in cometary samples runs counter to the general understanding that cometary OM originates in the cold interstellar molecular clouds, outer fringes of the solar nebula, or cold outer disk (Messenger 2000; Bockelée–Morvan et al. 2002; Remusat et al. 2009; Ciesla and Sandford 2012). It can be accounted for by the outward transportation of the high-temperature materials by turbulent radial mixing, where they accreted along with ice and OM to form the comets (Bockelée–Morvan et al. 2002; Ciesla 2007; Nakamura et al. 2008; Starkey and Franchi 2013). Subsequent to the accretion, Amberley3 OM was heated by transient events to gain the organic signature we observe today. Alternatively, it could be explained by radial inward (sunward) transportation of outer region materials by advection, turbulent diffusion, or gas drag (Bockelée–Morvan et al. 2002; Cuzzi and Weidenschilling 2006), where they were then thermally annealed.

CONCLUSIONS

With a possible link to ice-rich (cometary) parent bodies, most anhydrous CP-IDPs have avoided parent body processes, and thus, they are potentially the best samples that retain information about the primitive materials that were produced in the ISM, cold molecular cloud, and/or outer regions of the protoplanetary disk. However, while different IDPs have experienced various extents of atmospheric entry heating, cometary IDPs are among the most heated materials in light of their higher eccentricities and atmospheric entry velocities. In order to understand the nature of the primitive material that was present in IDPs, it is essential to systematically identify the heating they experienced during atmospheric entry and the effects this causes.

In this study, we have studied five anhydrous CP-IDPs (Rosslyn3, Drake3, Drake4, Balmoral3b, and Amberley3). The Drake particles are potentially derived from comet 26P/Grigg–Skjellerup, which has a sufficiently low eccentricity to deliver to the Earth dust particles at low atmospheric entry velocities and thus minimal heating. In order to fully account for the distribution, chemistry, structure, and isotopic compositions of the OM contained in the IDP samples, we have conducted a range of coordinated studies with Raman spectroscopy, SEM, and NanoSIMS.

The comparable Raman D band parameters between IDP and primitive chondritic OM indicate that their OM shares similar maturity via gaining sp^2 cluster/domain sizes. The similarity in the sp^2 cluster/domain sizes but disparity between their Γ_G values suggests the

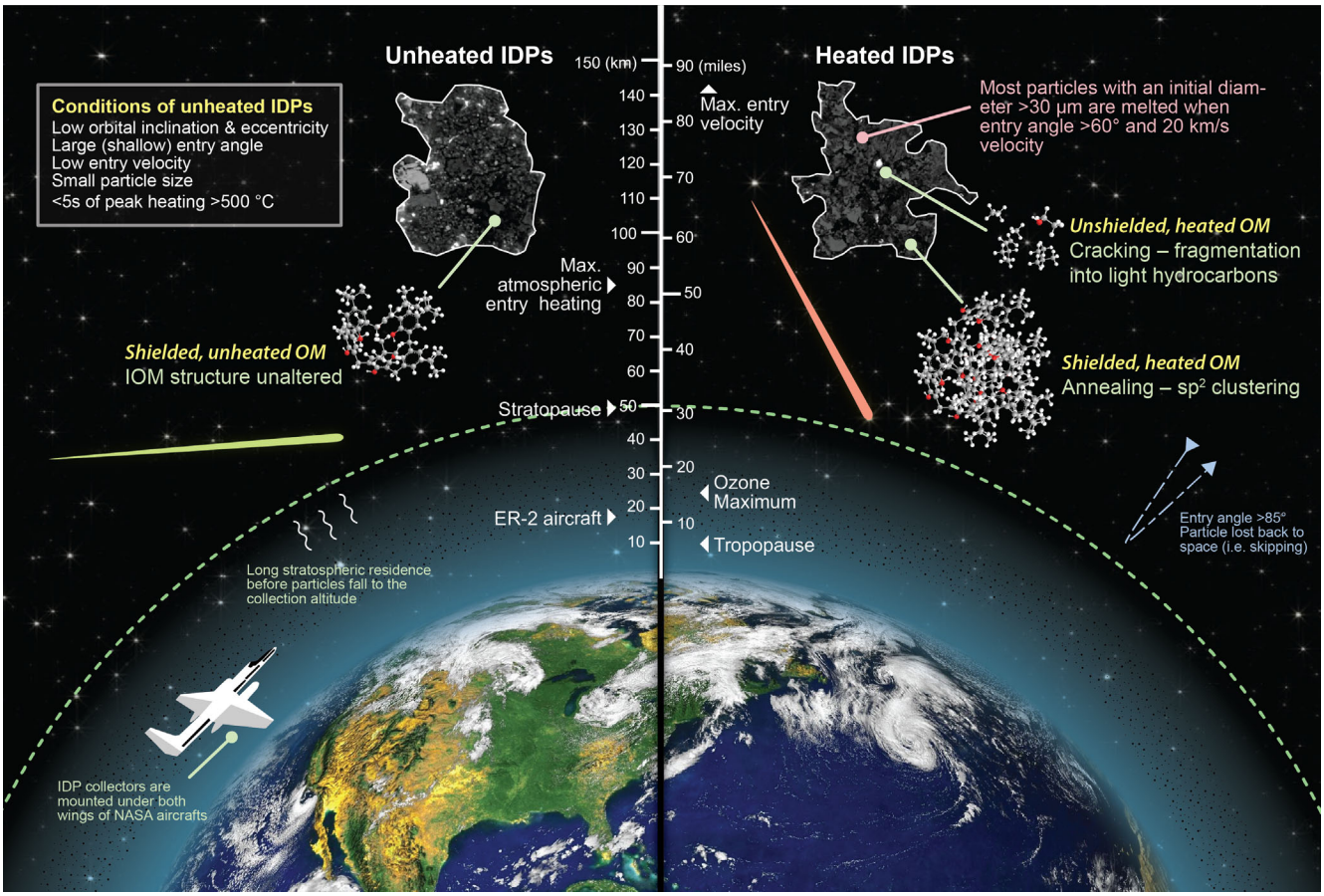

Fig. 13. Schematic diagram showing unheated and heated IDPs and the corresponding heating effect from atmospheric entry heating.

presence of different organic components comprising different non-aromatic sp^2 contents (e.g., olefin sp^2 C=C). The Γ_G widening in IDP OM indicates the development of crystalline domains without graphitic ordering, as large-scale graphitization would have significantly reduced the Γ_G value. The Raman band parameters (both D and G bands) of IDP OM are similar to that of the OM in Tagish Lake meteoritem which has been experimentally heated to simulate short duration heating. Amberley3 represents the most heated IDP sample analyzed in this study; the Raman parameters of its OM are comparable to the Tagish Lake meteorite OM experimentally heated to 600–900 °C. The similarities between the Raman D and G band parameters of IDP OM to that of experimentally heated Tagish Lake meteorite but not to other chondritic OM suggest that (1) IDP OM has been exposed to short-term heating, and/or (2) IDP OM has a unique organic structure that is different from chondritic OM.

We have observed a correlation between the elemental, chemical, and isotopic compositions of IDP OM. C-bearing components are more common in the fine-grained matrices of the IDPs, which offer a heat-shielding effect to prevent the OM from full-scale thermal decomposition. The less heated IDPs typically contain a larger proportion of pristine OM with smaller crystalline domains (aromatic units), higher heteroatom abundances (i.e., stronger fluorescence in their Raman spectra), higher δD and $\delta^{13}C$ values, but lower H/C ratios. The observation of a lower H/C ratio in less heated IDP is unexpected. It is because thermal annealing typically enhances aromaticity by converting the aliphatic sp^3 C into aromatic sp^2 C, leading to an increase in the size of the aromatic moieties and a reduction in the overall H/C ratio as observed for chondritic OM. A possible explanation for this is the presence of a significant proportion of disordered C with low H content, as the thermal decomposition of these low H materials would lead to a higher overall H/C ratio. We postulate that the C-rich material is made up of a large and complex network of C whereas the sp^2 sites occur as both non-aromatic contents such as olefinic components, as well as aromatic units of smaller

cluster/domain sizes, and a high proportion of sp^3 C–C with low H abundances and high oxygenated contents as bridging material occurring between the sp^2 sites.

Acknowledgments—We thank the NASA Cosmic Dust Laboratory for providing the IDP samples. We thank Larry Nittler and Timothy Jull for the editorial handling of this manuscript. This paper has benefited greatly from thorough and constructive comments of Henner Busemann and two anonymous reviewers. This study was supported by a Science and Technology Facilities Council (STFC) rolling grant (ST/L000776/1, ST/P000657/1). We acknowledge Lindsay Keller and Scott Messenger for their helpful advice provided on atmospheric entry heating of IDPs. We are grateful for the assistance from Pete Landsberg at the Open University for his help on preparing the terrestrial standards used in our NanoSIMS analysis, Gordon Imlach at the Open University, and Tomasz Goral at the Natural History Museum with FEG-SEM measurements. Finally, the authors dedicate this paper to the memory of Christine Floss and her significant contributions to our understanding of IDPs that made this work possible.

Editorial Handling—Dr. Larry Nittler

REFERENCES

Aikawa Y. and Herbst E. 2001. Two-dimensional distributions and column densities of gaseous molecules in protoplanetary disks. *Astronomy & Astrophysics* 371:1107–1117.

Aléon J., Engrand C., Robert F., and Chaussidon M. 2001. Clues to the origin of interplanetary dust particles from the isotopic study of their hydrogen-bearing phases. *Geochimica et Cosmochimica Acta* 65:4399–4412.

Aléon J., McKeegan K., and Leshin L. 2006. Oxygen isotopes in chondritic interplanetary dust: parent-bodies and nebular oxygen reservoirs (abstract #1921). 37th Lunar and Planetary Science Conference. CD-ROM.

Alexander C. M. O'D., Fogel M. L., Yabuta H., and Cody G. D. 2007. The origin and evolution of chondrites recorded in the elemental and isotopic compositions of their macromolecular organic matter. *Geochimica et Cosmochimica Acta* 71:4380–4403.

Alexander C. M. O'D., Cody G. D., Kebukawa Y., Bowden R., Fogel M. L., Kilcoyne A. L. D., Nittler L. R., and Herd C. D. K. 2014. Elemental, isotopic, and structural changes in Tagish Lake insoluble organic matter produced by parent body processes. *Meteoritics & Planetary Science* 49:503–525.

Alexander C. M. O. D., Cody G. D., De Gregorio B. T., Nittler L. R., and Stroud R. M. 2017. The nature, origin and modification of insoluble organic matter in chondrites, the major source of Earth's C and N. *Geochemistry* 77:227–256.

Anders E. 1989. Pre-biotic organic matter from comets and asteroids. *Nature* 342:255–257.

Antognozzi M., Sentimenti A., and Valdrè U. 1997. Fabrication of nano-tips by carbon contamination in a scanning electron microscope for use in scanning probe microscopy and field emission. *Microscopy Microanalysis Microstructures* 8:355–368.

Baratta G. A., Mennella V., Brucato J. R., Colangeli L., Leto G., Palumbo M. E., and Strazzulla G. 2004. Raman spectroscopy of ion-irradiated interplanetary carbon dust analogues. *Journal of Raman Spectroscopy* 35:487–496.

Baratta G. A., Brunetto R., Leto G., Palumbo M. E., Spinella F., and Strazzulla G. 2008. Raman spectroscopy of ion-irradiated astrophysically relevant materials. *Journal of Raman Spectroscopy* 39:211–219.

Bockelée–Morvan D., Gautier D., Hersant F., Huré J.-M., and Robert F. 2002. Turbulent radial mixing in the solar nebula as the source of crystalline silicates in comets. *Astronomy & Astrophysics* 384:1107–1118.

Boothroyd A. I. and Sackmann I. J. 1999. The CNO isotopes: Deep circulation in red giants and first and second dredge-up. *The Astrophysical Journal* 510:232–250.

Bradley J. P. 1994. Nanometer-scale mineralogy and petrography of fine-grained aggregates in anhydrous interplanetary dust particles. *Geochimica et Cosmochimica Acta* 58:2123–2134.

Bradley J. P. 2003. Interplanetary dust particles. In *Treatise on geochemistry*, edited by Holland H. D. and Turekian K. K. Oxford: Elsevier Pergamon. pp. 689–711.

Bradley J. P. and Brownlee D. E. 1986. Cometary particles: Thin sectioning and electron beam analysis. *Science* 231:1542–1544.

Bradley J. P., Brownlee D. E., and Fraundorf P. 1984. Discovery of nuclear tracks in interplanetary dust. *Science* 226:1432–1434.

Bradley J. P., Keller L. P., Brownlee D. E., and Thomas K. L. 1996. Reflectance spectroscopy of interplanetary dust particles. *Meteoritics & Planetary Science* 31:394–402.

Brown R. D. and Rice E. H. N. 1986. Galactochemistry—II. Interstellar deuterium chemistry. *Monthly Notices of the Royal Astronomical Society* 223:429–442.

Brownlee D. E., Joswiak D. J., Schlutter D. J., Pepin R. O., Bradley J. P., and Love S. G. 1995. Identification of individual cometary IDP's by thermally stepped He release (abstract #183). 26th Lunar and Planetary Science Conference. CD-ROM.

Brunetto R., Pino T., Dartois E., Cao A. T., d'Hendecourt L., Strazzulla G., and Bréchignac P. 2009. Comparison of the Raman spectra of ion irradiated soot and collected extraterrestrial carbon. *Icarus* 200:323–337.

Brunetto R., Borg J., Dartois E., Rietmeijer F. J. M., Grossemy F., Sandt C., Le Sergeant d'Hendecourt L., Rotundi A., Dumas P., Djouadi Z., and Jamme F. 2011. Mid-IR, Far-IR, Raman micro-spectroscopy, and FESEM–EDX study of IDP L2021C5: Clues to its origin. *Icarus* 212:896–910.

Brunetto R., Loeffler M. J., Nesvorný D., Sasaki S., and Strazzulla G. 2015. Asteroid surface alteration by space weathering processes. In *Asteroids IV*, edited by Michel P., DeMeo F. E., and Bottke W. F. Tucson, Arizona: University of Arizona Press. pp. 597–616.

Busemann H., Alexander C. M. O'D., and Nittler L. R. 2007. Characterization of insoluble organic matter in primitive

meteorites by microRaman spectroscopy. *Meteoritics & Planetary Science* 42:1387–1416.

Busemann H., Nguyen A. N., Cody G. D., Hoppe P., Kilcoyne A. L. D., Stroud R. M., Zega T. J., and Nittler L. R. 2009. Ultra-primitive interplanetary dust particles from the comet 26P/Grigg–Skjellerup dust stream collection. *Earth and Planetary Science Letters* 288:44–57.

Busemann H., Bajt S., Spring N. H., and Nittler L. R. 2011. Synchrotron Fourier transform infrared spectroscopy on fragments of interplanetary dust particles (IDPs) (abstract). *Meteoritics & Planetary Science* 74 (Suppl.):5506.

Butterworth A. L., Aballain O., Chappellaz J., and Sephton M. A. 2004. Combined element (H and C) stable isotope ratios of methane in carbonaceous chondrites. *Monthly Notices of the Royal Astronomical Society* 347:807–812.

Casiraghi C., Ferrari A. C., and Robertson J. 2005. Raman spectroscopy of hydrogenated amorphous carbons. *Physical Review B* 72:085401.

Champness P. 1970. Nucleation and growth of iron oxides in olivines, (Mg, Fe)2SiO_4. *Mineralogical Magazine* 37:790–800.

Chan Q. H. S., Zolensky M. E., Martinez J. E., Tsuchiyama A., and Miyake A. 2016. Magnetite plaquettes are naturally asymmetric materials in meteorites. *American Mineralogist* 101:2041–2050.

Chan Q. H. S., Zolensky M. E., Bodnar R. J., Farley C., and Cheung J. C. H. 2017. Investigation of organo-carbonate associations in carbonaceous chondrites by Raman spectroscopy. *Geochimica et Cosmochimica Acta* 201:392–409.

Chan Q. H. S., Zolensky M., Kebukawa Y., Fries M., Ito M., Steele A., Rahman Z., Nakato A., Kilcoyne A. L. D., Suga H., Takahashi Y., Takeichi Y., and Mase K. 2018. Organic matter in extraterrestrial water-bearing salt crystals. *Science Advances* 4:eaao3521.

Chan Q. H. S., Nakato A., Kebukawa Y., Zolensky M. E., Nakamura T., Maisano J. A., Colbert M. W., Martinez J. E., Kilcoyne A. L. D., Suga H., Takahashi Y., Takeichi Y., Mase K., and Wright I. P. 2019. Heating experiments of the Tagish Lake meteorite: Investigation of the effects of short-term heating on chondritic organics. *Meteoritics & Planetary Science* 54:104–125.

Charnley S. B., Tielens A. G. G. M., and Rodgers S. D. 1997. Deuterated methanol in the Orion compact ridge. *The Astrophysical Journal* 482:L203–L206.

Ciesla F. J. 2007. Outward transport of high-temperature materials around the midplane of the solar nebula. *Science* 318:613–615.

Ciesla F. J. and Sandford S. A. 2012. Organic synthesis via irradiation and warming of ice grains in the solar nebula. *Science* 336:452–454.

Clayton R. N. and Mayeda T. K. 1999. Oxygen isotope studies of carbonaceous chondrites. *Geochimica et Cosmochimica Acta* 63:2089–2104.

Clemett S. J., Maechling C. R., Zare R. N., Swan P. D., and Walker R. M. 1993. Identification of complex aromatic molecules in individual interplanetary dust particles. *Science* 262:721–725.

Cody G. D. and Alexander C. M. O'D. 2005. NMR studies of chemical structural variation of insoluble organic matter from different carbonaceous chondrite groups. *Geochimica et Cosmochimica Acta* 69:1085–1097.

Cody G. D., Alexander C. M. O. D., Yabuta H., Kilcoyne A. L. D., Araki T., Ade H., Dera P., Fogel M., Militzer B., and Mysen B. O. 2008. Organic thermometry for chondritic parent bodies. *Earth and Planetary Science Letters* 272:446–455.

Craig J. R. and Scott S. D. 1974. Sulfide phase equilibria. In *Sulfide mineralogy*, edited by Ribbe P. H. Washington, D.C.: Mineralogical Society of America. p. CS1-204.

Cuzzi J. N. and Weidenschilling S. J. 2006. Particle-gas dynamics and primary accretion. In *Meteorites and the early solar system II*, edited by Lauretta D. S. and McSween H. Y. Tucson, Arizona: University of Arizona Press. pp. 353–381.

Dartois E., Muñoz Caro G. M., Deboffle D., Montagnac G., and d'Hendecourt L. 2005. Ultraviolet photoproduction of ISM dust. *Astronomy & Astrophysics* 432:895–908.

Davidson J., Busemann H., and Franchi I. A. 2012. A NanoSIMS and Raman spectroscopic comparison of interplanetary dust particles from comet Grigg-Skjellerup and non-Grigg Skjellerup collections. *Meteoritics & Planetary Science* 47:1748–1771.

Derenne S. and Robert F. 2010. Model of molecular structure of the insoluble organic matter isolated from Murchison meteorite. *Meteoritics & Planetary Science* 45:1461–1475.

Dischler B., Bubenzer A., and Koidl P. 1983. Bonding in hydrogenated hard carbon studied by optical spectroscopy. *Solid State Communications* 48:105–108.

Ferini G., Baratta G. A., and Palumbo M. E. 2004. A Raman study of ion irradiated icy mixtures. *Astronomy & Astrophysics* 414:757–766.

Ferrari A. C. and Robertson J. 2000. Interpretation of Raman spectra of disordered and amorphous carbon. *Physical Review B* 61:14,095–14,107.

Floss C., Stadermann F. J., Bradley J. P., Dai Z. R., Bajt S., Graham G., and Lea A. S. 2006. Identification of isotopically primitive interplanetary dust particles: A NanoSIMS isotopic imaging study. *Geochimica et Cosmochimica Acta* 70:2371–2399.

Floss C., Stadermann F. J., Mertz A. F., and Bernatowicz T. J. 2010. A NanoSIMS and Auger nanoprobe investigation of an isotopically primitive interplanetary dust particle from the 55P/Tempel-Tuttle targeted stratospheric dust collector. *Meteoritics & Planetary Science* 45:1889–1905.

Flynn G. J. 1989. Atmospheric entry heating: A criterion to distinguish between asteroidal and cometary sources of interplanetary dust. *Icarus* 77:287–310.

Flynn G. J., Sutton S. R., Thomas K. L., Keller L. P., and Klöck W. 1992. Zinc depletions and atmospheric entry heating in stratospheric cosmic dust particles (abstract #375). 23rd Lunar and Planetary Science Conference. CD-ROM

Flynn G. J., Bajt S., Sutton S. R., Zolensky M. E., Thomas K. L., and Keller L. P. 1996. The abundance pattern of elements having low nebular condensation temperatures in interplanetary dust particles: Evidence for a new chemical type of chondritic material. *International Astronomical Union Colloquium* 150:291–294.

Flynn G. J., Keller L. P., Feser M., Wirick S., and Jacobsen C. 2003. The origin of organic matter in the solar system: Evidence from the interplanetary dust particles. *Geochimica et Cosmochimica Acta* 67:4791–4806.

Flynn G. J., Keller L. P., Jacobsen C., and Wirick S. 2004. An assessment of the amount and types of organic matter contributed to the Earth by interplanetary dust. *Advances in Space Research* 33:57–66.

Flynn G. J., Wirick S., and Keller L. P. 2013. Organic grain coatings in primitive interplanetary dust particles: Implications for grain sticking in the solar nebula. *Earth, Planets and Space* 65:13.

Flynn G. J., Keller L. P., Wirick S., Hu W., Li L., Yan H., Huang X., Nazaretski E., Lauer K., and Chu Y. S. 2016. High-nickel iron-sulfides in anhydrous, GEMS-rich IDPs (abstract). *Meteoritics & Planetary Science* 79:6205.

Fraundorf P., Lyons T., and Schubert P. 1982. The survival of solar flare tracks in interplanetary dust silicates on deceleration in the Earth's atmosphere. *Journal of Geophysical Research: Solid Earth* 87:A409–A412.

Gaydou M., Moragas T., Juliá-Hernández F., and Martin R. 2017. Site-selective catalytic carboxylation of unsaturated hydrocarbons with CO_2 and water. *Journal of the American Chemical Society* 139:12,161–12,164.

Germani M. S., Bradley J. P., and Brownlee D. E. 1990. Automated thin-film analyses of hydrated interplanetary dust particles in the analytical electron microscope. *Earth and Planetary Science Letters* 101:162–179.

Greshake A., Klöck W., Arndt P., Maetz M., Flynn G. J., Bajt S., and Bischoff A. 1998. Heating experiments simulating atmospheric entry heating of micrometeorites: Clues to their parent body sources. *Meteoritics & Planetary Science* 33:267–290.

Hart R. K., Kassner T. F., and Maurin J. K. 1970. The contamination of surfaces during high-energy electron irradiation. *The Philosophical Magazine* 21:453–467.

Hirsch P., Kässens M., Püttmann M., and Reimer L. 1994. Contamination in a scanning electron microscope and the influence of specimen cooling. *Scanning* 16:101–110.

Homma Y., Kouketsu Y., Kagi H., Mikouchi T., and Yabuta H. 2015. Raman spectroscopic thermometry of carbonaceous material in chondrites: Four-band fitting analysis and expansion of lower temperature limit. *Journal of Mineralogical and Petrological Sciences* 110:276–282.

Jackson A. A. and Zook H. A. 1992. Orbital evolution of dust particles from comets and asteroids. *Icarus* 97:70–84.

Jones A. P. 2012. Variations on a theme—The evolution of hydrocarbon solids. *Astronomy & Astrophysics* 540: A98.

Joswiak D. J., Brownlee D. E., Pepin R. O., and Schlutter D. J. 2007. Densities and mineralogy of cometary and asteroidal interplanetary dust particles collected in the stratosphere. Workshop on Dust in Planetary Systems, September 26–30, Kauai, Hawaii. pp. 141–144.

Joswiak D. J., Brownlee D. E., Matrajt G., Westphal A. J., and Snead C. J. 2009. Kosmochloric Ca-rich pyroxenes and FeO-rich olivines (Kool grains) and associated phases in Stardust tracks and chondritic porous interplanetary dust particles: Possible precursors to FeO-rich type II chondrules in ordinary chondrites. *Meteoritics & Planetary Science* 44:1561–1588.

Joswiak D. J., Brownlee D. E., Nguyen A. N., and Messenger S. 2017. Refractory materials in comet samples. *Meteoritics & Planetary Science* 52:1612–1648.

Juliá-Hernández F., Moragas T., Cornella J., and Martin R. 2017. Remote carboxylation of halogenated aliphatic hydrocarbons with carbon dioxide. *Nature* 545:84.

Keller L. P. and Messenger S. 2011. On the origins of GEMS grains. *Geochimica et Cosmochimica Acta* 75:5336–5365.

Keller L. P., Thomas K. L., and McKay D. S. 1992. An interplanetary dust particle with links to CI chondrites. *Geochimica et Cosmochimica Acta* 56:1409–1412.

Keller L. P., Thomas K. L., and McKay D. S. 1996. Mineralogical changes in IDPs resulting from atmospheric entry heating. In Astronomical Society of the Pacific Conference, Gainesville, FL, USA. pp. 295–298.

Keller L. P., Messenger S., Flynn G. J., Clemett S., Wirick S., and Jacobsen C. 2004. The nature of molecular cloud material in interplanetary dust. *Geochimica et Cosmochimica Acta* 68:2577–2589.

Kouketsu Y., Mizukami T., Mori H., Endo S., Aoya M., Hara H., Nakamura D., and Wallis S. 2014. A new approach to develop the Raman carbonaceous material geothermometer for low-grade metamorphism using peak width. *Island Arc* 23:33–50.

Kuebler K. E., Jolliff B. L., Wang A., and Haskin L. A. 2006. Extracting olivine (Fo–Fa) compositions from Raman spectral peak positions. *Geochimica et Cosmochimica Acta* 70:6201–6222.

Lahfid A., Beyssac O., Deville E., Negro F., Chopin C., and Goffé B. 2010. Evolution of the Raman spectrum of carbonaceous material in low-grade metasediments of the Glarus Alps (Switzerland). *Terra Nova* 22:354–360.

Lantz C., Brunetto R., Barucci M. A., Fornasier S., Baklouti D., Bourçois J., and Godard M. 2017. Ion irradiation of carbonaceous chondrites: A new view of space weathering on primitive asteroids. *Icarus* 285:43–57.

Love S. G. and Brownlee D. E. 1991. Heating and thermal transformation of micrometeoroids entering the Earth's atmosphere. *Icarus* 89:26–43.

Love S. G. and Brownlee D. E. 1993. A direct measurement of the terrestrial mass accretion rate of cosmic dust. *Science* 262:550–553.

Matrajt G., Brownlee D., Joswiak D., and Taylor S. 2005. Atmospheric entry heating effects on organic carbonaceous phases of IDPs and polar micrometeorites: An EEELS study (abstract #1553). 36th Annual Lunar and Planetary Science Conference. CD-ROM.

Matrajt G., Brownlee D., Sadilek M., and Kruse L. 2006. Survival of organic phases in porous IDPs during atmospheric entry: A pulse-heating study. *Meteoritics & Planetary Science* 41:903–911.

Matrajt G., Messenger S., Brownlee D., and Joswiak D. 2012. Diverse forms of primordial organic matter identified in interplanetary dust particles. *Meteoritics & Planetary Science* 47:525–549.

Matsuhisa Y., Goldsmith J. R., and Clayton R. N. 1979. Oxygen isotopic fractionation in the system quartz-albite-anorthite-water. *Geochimica et Cosmochimica Acta* 43:1131–1140.

McKeegan K. D., Kallio A. P. A., Heber V. S., Jarzebinski G., Mao P. H., Coath C. D., Kunihiro T., Wiens R. C., Nordholt J. E., Moses R. W., Reisenfeld D. B., Jurewicz A. J. G., and Burnett D. S. 2011. The oxygen isotopic composition of the Sun inferred from captured solar wind. *Science* 332:1528–1532.

Messenger S. 2000. Identification of molecular-cloud material in interplanetary dust particles. *Nature* 404:968–971.

Messenger S. 2002. Opportunities for the stratospheric collection of dust from short-period comets. *Meteoritics & Planetary Science* 37:1491–1505.

Messenger S., Stadermann F. J., Floss C., Nittler L. R., and Mukhopadhyay S. 2003. Isotopic signatures of presolar materials in interplanetary dust. *Space Science Reviews* 106:155–172.

Messenger S., Keller L., Nakamura-Messenger K., and Ito M. 2007. The abundance and distribution of presolar materials in cluster IDPs (abstract #2122). 38th Lunar and Planetary Science Conference. CD-ROM.

Messenger S., Nakamura-Messenger K., and Keller L. P. 2008. ^{15}N-rich organic globules in a cluster IDP and the Bells CM2 chondrite (abstract #2391). 39th Lunar and Planetary Institute Science Conference.

Messenger S., Keller L., Nakamura-Messenger K., Nguyen A., and Walker R. M. 2009. Stardust abundance variations among interplanetary dust particles (abstract). *Meteoritics & Planetary Science* 72:5357.

Messenger S. R., Keller L., and Nakamura-Messenger K. 2010. History of nebular processing traced by silicate stardust in IDPs (abstract #2483). 41st Lunar and Planetary Science Conference. CD-ROM.

Millar T. J., Bennett A., and Herbst E. 1989. Deuterium fractionation in dense interstellar clouds. *The Astrophysical Journal* 340:906.

Muñoz Caro G. M., Matrajt G., Dartois E., Nuevo M., d'Hendecourt L., Deboffle D., Montagnac G., Chauvin N., Boukari C., and Le Du D. 2006. Nature and evolution of the dominant carbonaceous matter in interplanetary dust particles: Effects of irradiation and identification with a type of amorphous carbon. *Astronomy & Astrophysics* 459:147–159.

Muñoz Caro G. M., Rietmeijer F. J. M., Souza-Egipsy V., and Valles-González M. P. 2012. A potentially new type of nonchondritic interplanetary dust particle with hematite, organic carbon, amorphous Na,Ca-aluminosilicate, and FeO-spheres. *Meteoritics & Planetary Science* 47:248–261.

Nakamura T. 2005. Post-hydration thermal metamorphism of carbonaceous chondrites. *Journal of Mineralogical and Petrological Sciences* 100:260–272.

Nakamura K., Messenger S., and Keller L. 2005. TEM and NanoSIMS study of hydrated/anhydrous phase mixed IDPs: cometary or asteroidal origin? (abstract #1824). 36th Lunar and Planetary Science Conference. CD-ROM.

Nakamura T., Noguchi T., Tsuchiyama A., Ushikubo T., Kita N. T., Valley J. W., Zolensky M. E., Kakazu Y., Sakamoto K., Mashio E., Uesugi K., and Nakano T. 2008. Chondrulelike objects in short-period comet 81P/Wild 2. *Science* 321:1664–1667.

Nakamura-Messenger K., Messenger S., Keller L. P., Clemett S. J., and Zolensky M. E. 2006. Organic globules in the Tagish Lake meteorite: Remnants of the protosolar disk. *Science* 314:1439–1442.

Nakamura-Messenger K., Clemett S. J., Messenger S., and Keller L. P. 2011. Experimental aqueous alteration of cometary dust. *Meteoritics & Planetary Science* 46:843–856.

Nakamura-Messenger K., Herzog G., Smith T., Keller L., Flynn G., Khodja H., Taylor S., Wirick S., and Messenger S. 2012. Coordinated analyses of mineral-organic matter associations in interplanetary dust particles (abstract). *Meteoritics & Planetary Science* 75:5325.

Nittler L. R., Alexander C. M. O'D., Gao X., Walker R. M., and Zinner E. 1997. Stellar sapphires: The properties and origins of presolar Al_2O_3 in meteorites. *The Astrophysical Journal* 483:475.

Österle W., Giovannozzi A., Gradt T., Häusler I., Rossi A., Wetzel B., Zhang G., and Dmitriev A. I. 2015. Exploring the potential of Raman spectroscopy for the identification of silicone oil residue and wear scar characterization for the assessment of tribofilm functionality. *Tribology International* 90:481–490.

Pizzarello S. and Holmes W. 2009. Nitrogen-containing compounds in two CR113 meteorites: 15N composition, molecular distribution and precursor molecules. *Geochimica et Cosmochimica Acta* 73:2150–2162.

Pizzarello S., Cooper G., and Flynn G. J. 2006. The nature and distribution of the organic material in Carbonaceous chondrites and interplanetary dust particles. In *Meteorites and the early solar system II*, edited by Lauretta D. S. and McSween H. Y. Jr. Tucson, Arizona: University of Arizona Press. pp. 625–651.

Quirico E., Raynal P.-I., and Bourot-Denise M. 2003. Metamorphic grade of organic matter in six unequilibrated ordinary chondrites. *Meteoritics & Planetary Science* 38:795–811.

Quirico E., Borg J., Raynal P.-I., Montagnac G., and d'Hendecourt L. 2005. A micro-Raman survey of 10 IDPs and 6 carbonaceous chondrites. *Planetary and Space Science* 53:1443–1448.

Quirico E., Montagnac G., Rouzaud J. N., Bonal L., Bourot-Denise M., Duber S., and Reynard B. 2009. Precursor and metamorphic condition effects on Raman spectra of poorly ordered carbonaceous matter in chondrites and coals. *Earth and Planetary Science Letters* 287:185–193.

Raynal P., Quirico E., Borg J., and D'Hendecourt L. 2001. Micro-Raman survey of the carbonaceous matter in stratospheric IDPs and carbonaceous chondrites. *Meteoritics & Planetary Science Supplement* 36:A171.

Remusat L., Robert F., Meibom A., Mostefaoui S., Delpoux O., Binet L., Gourier D., and Derenne S. 2009. Protoplanetary disk chemistry recorded by D-rich organic radicals in carbonaceous chondrites. *The Astrophysical Journal* 698:2087–2092.

Rietmeijer F. J. M. 1991. Aqueous alteration in five chondritic porous interplanetary dust particles. *Earth and Planetary Science Letters* 102:148–157.

Rietmeijer F. J. M. 1996. Cellular precipitates of iron oxide in olivine in a stratospheric interplanetary dust particle. *Mineralogical Magazine* 60:877–885.

Rietmeijer F. J. M. 2004. Dynamic pyrometamorphism during atmospheric entry of large (~10 micron) pyrrhotite fragments from cluster IDPs. *Meteoritics & Planetary Science* 39:1869–1887.

Robert F. 2002. Water and organic matter D/H ratios in the solar system: A record of an early irradiation of the nebula? *Planetary and Space Science* 50:1227–1234.

Robertson J. 2002. Diamond-like amorphous carbon. *Materials Science and Engineering: R: Reports* 37:129–281.

Rotundi A., Ferrini G., Baratta G. A., Palumbo M. E., Palomba E., and Colangeli L. 2007. Combined micro-infrared (IR) and micro-Raman measurements on stratospheric interplanetery dust particles. *Workshop on Dust in Planetary Systems*, September 26–30, Kauai, Hawaii. pp. 149–153.

Rotundi A., Baratta G. A., Borg J., Brucato J. R., Busemann H., Colangeli L., D'Hendecourt L., Djouadi Z., Ferrini G., Franchi I. A., Fries M., Grossemy F., Keller L. P., Mennella V., Nakamura K., Nittler L. R., Palumbo M. E., Sandford S. A., Steele A., and Wopenka B. 2008. Combined micro-Raman, micro-infrared, and field emission scanning electron microscope analyses of comet 81P/Wild 2 particles collected by Stardust. *Meteoritics & Planetary Science* 43:367–397.

Sadezky A., Muckenhuber H., Grothe H., Niessner R., and Pöschl U. 2005. Raman microspectroscopy of soot and related carbonaceous materials: Spectral analysis and structural information. *Carbon* 43:1731–1742.

Sandford S. A. and Bradley J. P. 1989. Interplanetary dust particles collected in the stratosphere: Observations of atmospheric heating and constraints on their interrelationship and sources. *Icarus* 82:146–166.

Sandford S. A. and Walker R. M. 1985. Laboratory infrared transmission spectra of individual interplanetary dust particles from 2.5 to 25 microns. *The Astrophysical Journal* 291:838–851.

Sandford S. A., Bernstein M. P., and Dworkin J. P. 2001. Assessment of the interstellar processes leading to deuterium enrichment in meteoritic organics. *Meteoritics & Planetary Science* 36:1117–1133.

Schrader D. L., Davidson J., and McCoy T. J. 2016. Widespread evidence for high-temperature formation of pentlandite in chondrites. *Geochimica et Cosmochimica Acta* 189:359–376.

Schramm L. S., Brownlee D. E., and Wheelock M. M. 1989. Major element composition of stratospheric micrometeorites. *Meteoritics* 24:99–112.

Sephton M. A. and Botta O. 2005. Recognizing life in the Solar System: Guidance from meteoritic organic matter. *International Journal of Astrobiology* 4:269–276.

Shebanova O. N. and Lazor P. 2003. Raman spectroscopic study of magnetite ($FeFe_2O_4$): A new assignment for the vibrational spectrum. *Journal of Solid State Chemistry* 174:424–430.

Stadermann F. J., Floss C., and Wopenka B. 2006. Circumstellar aluminum oxide and silicon carbide in interplanetary dust particles. *Geochimica et Cosmochimica Acta* 70:6168–6179.

Starkey N. A. and Franchi I. A. 2013. Insight into the silicate and organic reservoirs of the comet forming region. *Geochimica et Cosmochimica Acta* 105:73–91.

Starkey N. A., Franchi I. A., and Alexander C. M. O. D. 2013. A Raman spectroscopic study of organic matter in interplanetary dust particles and meteorites using multiple wavelength laser excitation. *Meteoritics & Planetary Science* 48:1800–1822.

Starkey N. A., Franchi I. A., and Lee M. R. 2014. Isotopic diversity in interplanetary dust particles and preservation of extreme ^{16}O-depletion. *Geochimica et Cosmochimica Acta* 142:115–131.

Strazzulla G., Baratta G. A., and Palumbo M. E. 2001. Vibrational spectroscopy of ion-irradiated ices. *Spectrochimica Acta Part A: Molecular and Biomolecular Spectroscopy* 57:825–842.

Suttle M. D., Genge M. J., Folco L., and Russell S. S. 2017. The thermal decomposition of fine-grained micrometeorites, observations from mid-IR spectroscopy. *Geochimica et Cosmochimica Acta* 206:112–136.

Terzieva R. and Herbst E. 2000. The possibility of nitrogen isotopic fractionation in interstellar clouds. *Monthly Notices of the Royal Astronomical Society* 317:563–568.

Thomas K. L., Blanford G. E., Keller L. P., Klöck W., and McKay D. S. 1993. Carbon abundance and silicate mineralogy of anhydrous interplanetary dust particles. *Geochimica et Cosmochimica Acta* 57:1551–1566.

Thomas K. L., Keller L. P., Blanford G. E., and McKay D. S. 1994. Quantitative analyses of carbon in anhydrous and hydrated interplanetary dust particles. *AIP Conference Proceedings* 310:165–172.

Thomas K. L., Blanford G. E., Clemett S. J., Flynn G. J., Keller L. P., Klöck W., Maechling C. R., Mc Kay D. S., Messenger S., Nier A. O., Schlutter D. J., Sutton S. R., Warren J. L., and Zare R. N. 1995. An asteroidal breccia: The anatomy of a cluster IDP. *Geochimica et Cosmochimica Acta* 59:2797–2815.

Toppani A., Libourel G., Engrand C., and Maurette M. 2001. Experimental simulation of atmospheric entry of micrometeorites. *Meteoritics & Planetary Science* 36:1377–1396.

Tuinstra F. and Koenig J. L. 1970. Raman spectrum of graphite. *Journal of Chemical Physics* 53:1126–1130.

Ungerer P., Collell J., and Yiannourakou M. 2015. Molecular modeling of the volumetric and thermodynamic properties of kerogen: Influence of organic type and maturity. *Energy & Fuels* 29:91–105.

Vernazza P., Marsset M., Beck P., Binzel R. P., Birlan M., Brunetto R., Demeo F. E., Djouadi Z., Dumas C., Merouane S., Mousis O., and Zanda B. 2015. Interplanetary dust particles as samples of icy asteroids. *The Astrophysical Journal* 806:204.

Wang Y., Alsmeyer D. C., and McCreery R. L. 1990. Raman spectroscopy of carbon materials: Structural basis of observed spectra. *Chemistry of Materials* 2:557–563.

Weck P. F., Kim E., Wang Y., Kruichak J. N., Mills M. M., Matteo E. N., and Pellenq R. J. M. 2017. Model representations of kerogen structures: An insight from density functional theory calculations and spectroscopic measurements. *Scientific Reports* 7:7068.

Wooden D., Desch S., Harker D., Gail H.-P., and Keller L. 2007. Comet grains and implications for heating and radial mixing in the protoplanetary disk. In *Protostars and planets V*, edited by Reipurth B., Jewitt D., and Keil K. Tucson, Arizona: University of Arizona Press. pp. 815–833.

Wopenka B. 1988. Raman observations on individual interplanetary dust particles. *Earth and Planetary Science Letters* 88:221–231.

Wopenka B. and Pasteris J. D. 1993. Structural characterization of kerogens to granulite-facies graphite: Applicability of Raman microprobe spectroscopy. *The American Mineralogist* 78:533–557.

Yabuta H., Alexander C. M. O'D., Fogel M. L., Kilcoyne A. L. D., and Cody G. D. 2010. A molecular and isotopic study of the macromolecular organic matter of the ungrouped C2 WIS 91600 and its relationship to Tagish Lake and PCA 91008. *Meteoritics & Planetary Science* 45:1446–1460.

Yang Y., and Lee J.-W. 2019. Toward ideal carbon dioxide functionalization. *Chemical Science* 10:3905–3926.

Young E. D. and Russell S. S. 1998. Oxygen reservoirs in the early solar nebula inferred from an Allende CAI. *Science* 282:452–455.

Zolensky M. E. and Lindstrom D. J. 1992. Mineralogy of 12 large "chondritic" interplanetary dust particles. *Proceedings of Lunar and Planetary Science* 22:161–169.

Zolensky M. E. and Thomas K. L. 1995. Iron and iron-nickel sulfides in chondritic interplanetary dust particles. *Geochimica et Cosmochimica Acta* 59:4707–4712.

Zolensky M., Barrett R., and Browning L. 1993. Mineralogy and composition of matrix and chondrule rims in carbonaceous chondrites. *Geochimica et Cosmochimica Acta* 57:3123–3148.

Zolensky M. E., Zega T. J., Yano H., Wirick S., Westphal A. J., Weisberg M. K., Weber I., Warren J. L., Velbel M. A., Tsuchiyama A., Tsou P., Toppani A., Tomioka N., Tomeoka K., Teslich N., Taheri M., Susini J., Stroud R., Stephan T., Stadermann F. J., Snead C. J., Simon S. B., Simionovici A., See T. H., Robert F., Rietmeijer F. J. M., Rao W., Perronnet M. C., Papanastassiou D. A., Okudaira K., Ohsumi K., Ohnishi I., Nakamura-Messenger K., Nakamura T., Mostefaoui S., Mikouchi T., Meibom A., Matrajt G., Marcus M. A., Leroux H., Lemelle L., Le L., Lanzirotti A., Langenhorst F., Krot A. N., Keller L. P., Kearsley A. T., Joswiak D., Jacob D., Ishii H., Harvey R., Hagiya K., Grossman L., Grossman J. N., Graham G. A., Gounelle M., Gillet P., Genge M. J., Flynn G., Ferroir T., Fallon S., Ebel D. S., Dai Z. R., Cordier P., Clark B., Chi M., Butterworth A. L., Brownlee D. E., Bridges J. C., Brennan S., Brearley A., Bradley J. P., Bleuet P., Bland P. A., and Bastien R. 2006. Mineralogy and petrology of comet 81P/Wild 2 nucleus samples. *Science* 314:1735–1739.

SUPPORTING INFORMATION

Additional supporting information may be found in the online version of this article.

Fig. S1. Peak fitting on a Raman spectrum collected from spot analysis of Amberley3. (+): Background-corrected data. (a) Comparison between the fitting results of different curve fitting models. Coefficient of determination (r^2) values of the models are: LBWF: 0.9966; 2 Voigt: 0.9955; 2 Lorentzian: 0.9940; 2 Gaussian: 0.9951; 5 Lorentzian (one G and four D bands): 0.9970. (b) The LBWF curve-fitting model of the fitted spectrum (blue) and the decomposed D (green) and G (red) bands.

Fig. S2. Intra-particle comparison of the C Raman band parameters of the OM in the IDP samples. R^2 values determine how closely the data conform to the trendlines.

Fig. S3. Example of a two-Lorentzian fit performed on the Raman spectrum of the olivine in Rosslyn3. The middle plot shows that the fluorescence background has been subtracted from the raw spectrum assuming a linear baseline between 750 and 900 cm^{-1}. Minimal misfit was observed as displayed by the residual spectrum.

Fig. S4. C contamination on sample Rosslyn3 after electron irradiation.

Fig. S5. Raman peak parameters of D and G bands of selected spectra of the IDP samples (●: Rosslyn3, ▼: Drake3, ▲: Drake4, ◀: Balmoral3b, and ▶: Amberley3) collected at different stages of the analytical sequence. Black markers—spectra obtained while IDP grains were still on the NASA glass slides; Blue markers —after samples were pressed flat into gold foil prior to any analysis; Red markers—the flattened IDPs have been exposed to electron beam during FEG-SEM analysis.

Table S1. *T*-tests (*P*-values), significance level (α) = 0.05. If the *P*-value is smaller than α, then we reject the null hypothesis of equal averages, and conclude that there is a statistically significant difference.

Table S2. Analytical area and number of planes acquired by NanoSIMS analysis.

Table S3. Isotopic compositions of terrestrial standard materials.

Table S4. Elemental abundances (at%) of the IDPs measured using EDX analysis.